Repeatability and Intermediate Precisions of the CPMA-Electrometer System

by

Jordan Taylor Faust Titosky

A thesis submitted in partial fulfillment of the requirements for the degree of

Master of Science

Department of Mechanical Engineering
University of Alberta

Abstract

The centrifugal particle mass analyzer (CPMA)-electrometer system has been proposed as an alternative method of calibration for devices that measure black carbon. This system is proposed to replace the current calibration standard of NIOSH 5040. The repeatability and intermediate precision of the CPMA-electrometer was determined through a series of experiments that examined an individual components of the system to determine the overall expected level of variation of the system. The key measurement components of this measurement system include the CPMA, a Faraday cup, an electrometer and a flow controller. These devices work together to classify a charged aerosol for a specific mass to charge ratio, capture the charge, and measure the current flow.

Two devices were compared to a known standard, the electrometer and the flow controller. Though these tests it was found the flow controller had an accuracy of less than 1%, a repeatability of less than 0.4% and an M=2 intermediate precision of 0.3% while the electrometer has a bias error of 2%. The Faraday cups were testing using the two Faraday cup-electrometer systems in parallel. Measurements were collected on both devices simultaneously where the repeatability was found to be less than 0.8% for the majority of tests, and an M=2intermediate precision of 2.2%.

The CPMA was tested using a tandem CPMA-CPMA experiment where one device classified the particles to a known set point and the second device scanned across a range of values to determine the peak value. Data was normalized by the initial set point on the first device. Through this it was found the CPMA had an average repeatability of 0.8% while the M=2 intermediate precision was 1.3%.

Using these intermediate precisions an estimate of the overall systems intermediate precision was calculated as 2.6%. Tests were also conducted on the CPMA-electrometer system where comparison measurements were collected on a challenge instrument. Between measurements that were collected across a number of days it was found a repeat calibration tests were likely to have less than 5% variation, a great improvement over NIOSH 5040 and a comparable result to the calculated intermediate precision.

Preface

I completed the majority of construction of the experimental setup, data collection, and data analysis with assistance from the National Research Council of Canada, in Ottawa. The electrometer calibration was completed by technicians at the National Research Council of Canada. Manuscript composition was completed by myself with assistance and edits from Dr. Olfert. Chapter 1 and 5 are my original work.

Acknowledgements

I would like to thank Dr. Olfert for his help and support with this project. His new ideas for possible experiments and data analysis techniques were incredibly helpful. I would also like to thank Dr. Olfert for providing me the opportunity to travel to Ottawa and work with the National Research Council of Canada.

I would like to thank the individuals at the National Research Council of Canada in Ottawa that assisted with experimentation while I was at their facility.

Lastly, I would like to thank my family and friends. It was their continual support and kept me moving forward with a level head. They have been there for me along this entire journey, and I would not be where I am today without them.

Table of Contents

List of Tables

List of Figures

List of Variables

A	Area of the transfer function
B_i	Mobility of a particle of mass m_i
d	Diameter of particle
e	Elementary charge (1.602 x 10^{-19} C)
$FWHM$	Full width half maximum of transfer function
h	Height of transfer function as instrument set point
I	Measured Current
λ	Parameter that modifies the amplitude of the CPMA transfer function
M_{+1}	Mass set point of the CPMA
m	An arbitrary mass
$m_{\max}$	Maximum mass that is able to pass though the CPMA
m_{total}	The total mass that has passed though the system
m_0	The mass of uncharged particles
N_1	The particle count exiting CPMA 1
N_2	The particle count exiting CPMA 2
n_i	The number of particles with i charges
n_q	The number of charges on a particle
Q	Volume flow rate
R_s	The reflectance of a sample
R_m	The resolution of the CPMA
R_w	The reflectance of a blank filter
r_c	The center radius between the two CPMA cylinders
r_{inner}	The radius of the inner CPMA cylinder
r_{outer}	The radius of the outer CPMA cylinder
SN'	The smoke number of an individual sample
μ	Parameter that modifies the width of the CPMA transfer function
V	The voltage between the two cylinders of the CPMA
ψ	Parameter that modifies the mass setpoint of the CPMA

ω_c	The rotational speed of the CPMA at radius r_c
Ω	The transfer function of the CPMA

List of Acronyms

AFM	Aerosol Flow Meter
APM	Aerosol Particle Mass Analyzer
ARP	Aerospace Recommended Pratice
Atm	Atmospheres
BC	Black Carbon
BNC	Bayonet Neill-Concelman
CH_4	Methane
CO	Carbon Monoxide
CO_2	Carbon Dioxide
CPC	Condensation Particle Counter
CPMA	Centrifugal Particle Mass Analyser
DMA	Differential Mobility Analyzer
DOS	bis(2-ethylhexyl) sebacate
EC	Elemental Carbon
HEPA	High Efficiency Particulate Air
H_2O	Water
LII	Laser-Induced Incandescence
LPM	Liters Per Minute
MSS	Micro-Soot Sensor
NIOSH	National Institute for Occupational Safety and Health
NOx	Nitrous Oxides
NRC	National Research Council of Canada
nvPMmi	Non-Volatile Particulate Matter Mass Instrument
nvPMni	Non-Volatile Particulate Matter Number Instrument
OC	Organic Carbon
$PM_{2.5}$	Particulate Matter smaller than 2.5 µm
SAE	Society of Automotive Engineers
SLPM	Standard Liters Per Minute
SN	Smoke Number

SOx	Sulfur Oxides
St. Dev	Standard Deviation
UDAC	Unipolar Diffusion Aerosol Charger
UofA	University of Alberta

Chapter 1 Introduction

Air travel has become a common method to transport both people and goods long distances in much shorter periods of time than previously possible. This marvel in technology has come with one major drawback, pollution. As with the majority of combustion engines, the common products of operation are carbon dioxide (CO_2), carbon monoxide (CO), organic carbon (OC), black carbon (BC, it is also known as elemental carbon, EC), water (H_2O), nitrous oxide products (NOx) and sulphur oxides (SOx) (Čokorilo 2016). The majority of these are released as gasses, however, black carbon is released as aerosol and organic carbon can be either an aerosol, or a gas. Black carbon is primarily composed of solid carbon, while organic carbon is the group that includes other forms of carbon compounds, such as unburned hydrocarbons.

Current estimations for the aircraft fleet average black carbon emission factor is 0.093g/kg_{fuel} in 2005 (i.e. this is the mass of black carbon produced per mass of fuel burnt). This is from landing and takeoff (fleet average black carbon emission factor of 0.147 g/kg_{fuel}) and cruising (fleet average black carbon emission factor of 0.088 g/kg_{fuel}) (Stettler et al. 2013). Depending on the type of engine, the individual ranges for measured black carbon emission factor range from 0.010 ± 0.003 g/kg_{fuel} to 0.500 ± 0.100 g/kg_{fuel}. These production values are given independent of particle size, an important aspect for particles for both climate and health purposes.

1.1 Climate effects of aerosols

Aerosols in the atmosphere have two main effects on climate. When light strikes the small particles present in an aerosol one of two things happens: the light is absorbed or the light is scattered. These effects are dependent on the coefficients of scattering and absorption (Magi et

al. 2005; Seinfeld and Pandis 2006), which are themselves based around the particle refractive index, chemical composition, and how different particle materials are mixed together (the mixing state). By examining these coefficients, it can be determined if an aerosol will have a net cooling effect, or net warming effect.

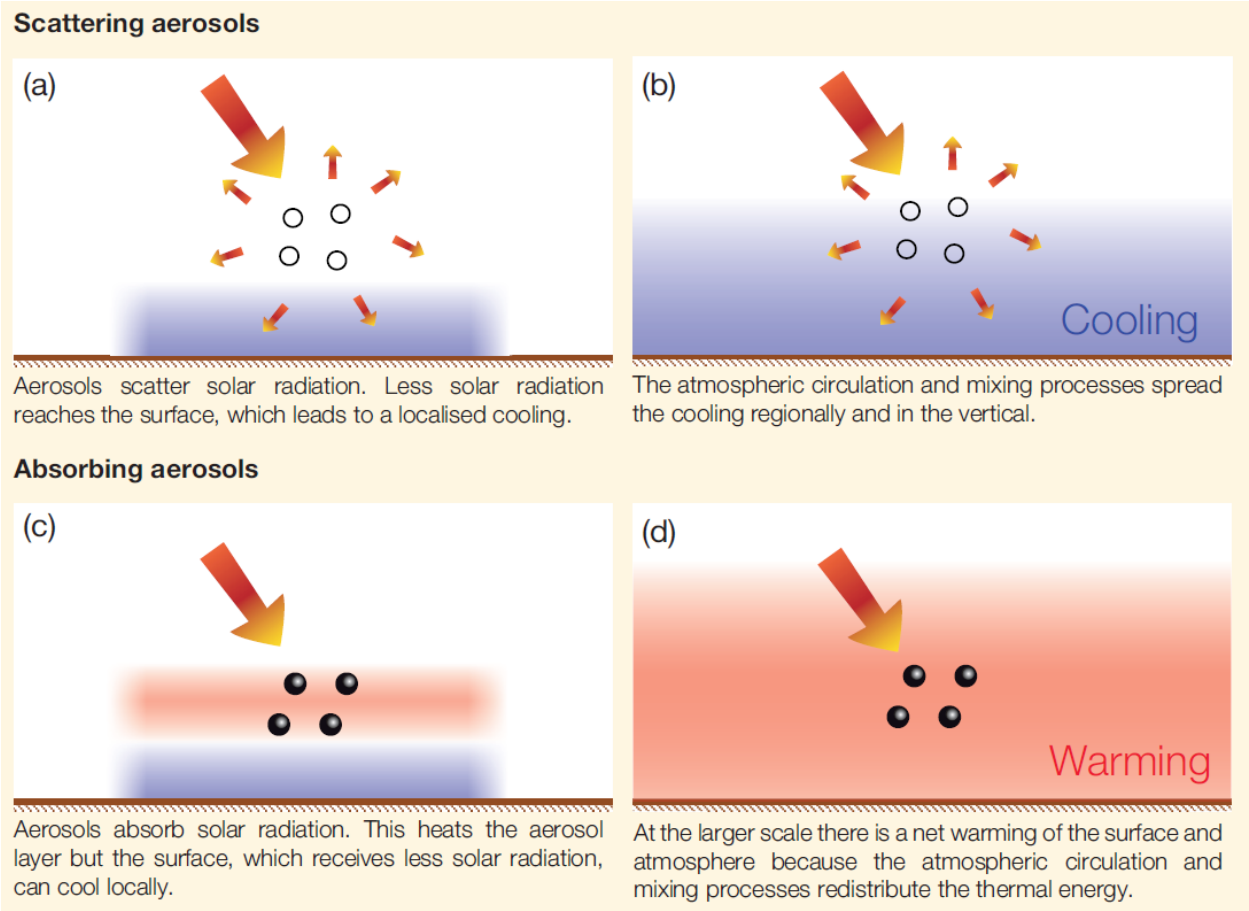

Figure 1.1: Effects of aerosols on light. Aerosols can have a net warming or cooling effect. Images a) and c) display the aerosols effect on light either scattering or absorbing it, while b) and d) display how this affects the local climate. (Boucher et al. 2013)

Most aerosols have a negative net radiative forcing i.e. a net cooling effect (Boucher et al. 2013). When photons strike the particles they are released in various directions, some of which travels to the Earth's surface, while others are reflected away from the planet (Magi et al. 2005). As such, the overall effect is less sunlight reaching the surface of the Earth, which causes localized cooling (as shown in Figure 1.1a and b). Black carbon exhibits the opposite effect of

most aerosols, rather than scattering the majority of light that strikes it, it absorbs the light. This absorption of the photon energy causes the temperature of the particles to increase, which causes an increase in the temperature of the atmosphere as can be seen in Figure 1.1c. Over time, the region of warmer air is mixed causing a new warming of the Earth's surface; this effect is displayed by the positive radiative forcing of black carbon of roughly +0.4 W/m^2 (Boucher et al. 2013). Figure 1.2 displays the net radiative force of various aerosols and gasses, within this figure the positive radiative forcing of black carbon is displayed and incudes the effects of black carbon on snow in addition to aerosolized black carbon. Comparatively, CO_2 has a radiative forcing of 1.68 W/m^2 and CH_4 (methane) has a radiative forcing of 0.97 W/m^2. These are two other products released from the combustion of fossil fuels. As such, a reduction in black carbon emissions from the burning of fossil fuels will help to slow climate change[1].

[1] Other methods to help reduce the effects of climate change through the use of aerosols cooling effects. Some research has suggested that injecting aerosols into the high atmosphere could help to counteract the effects of global warming (Crutzen 2006; Keith 2013). However, individuals are skeptical about this strategy as long term negative effects are possible such as the degradation of the ozone layer (Tilmes, Bee, and Salawitch 2008). This would allow more UV radiation to reach the earth surface in regions where the ozone layer is thinner. This effect would be slightly offset by the increase scattering effects and light absorption of the injected aerosol. While overall it is expected this would have a net cooling effect that would be equivalent to the warming effect caused by a doubling of atmospheric CO2, technologies or biological processes that rely on light from the sun would not be as effecting (Boucher et al. 2013). These include power production from solar energy, or photosynthesis in plants. Having lower production from solar panels would mean the decrease in energy production would have to be made up from another method, which with current trends in north America, would likely be through the burning of fossil fuels, which would only further the need for geoengineering. As such, stricter standards are required to help slow climate change.

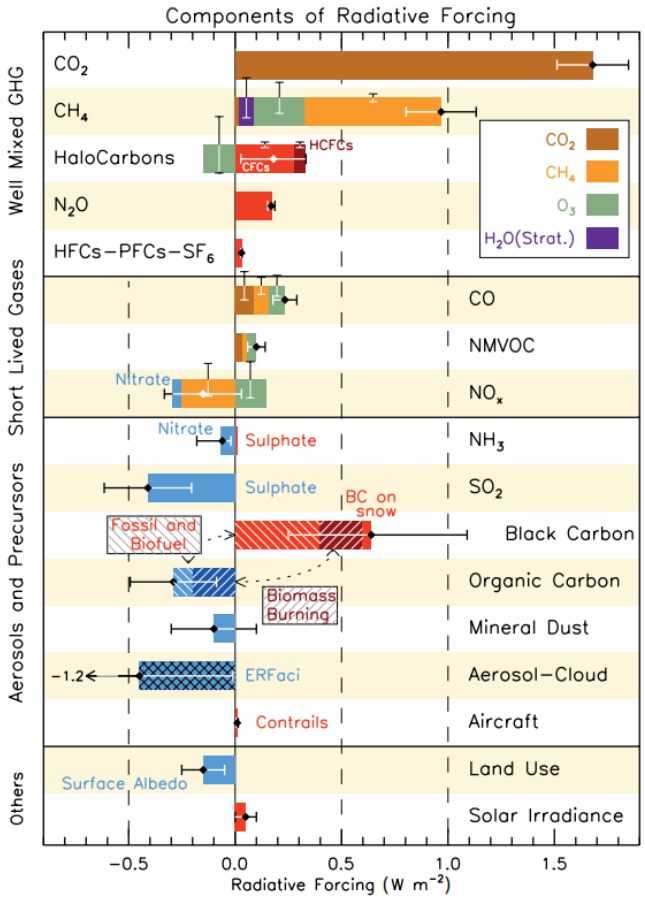

Figure 1.2: Radiative forcing of various aerosols and gases. (Myhre et al. 2013)

1.2 Health effects of black carbon

In 2015 it is estimated that 6.5 million deaths globally were caused by various forms of air pollution with 4.2 million caused by ambient particulates (Steel 2016). This is an astounding number as the total number of estimated deaths from all forms of pollution is only 9 million per year (Landrigan et al. 2017). This puts deaths due to particulates above the common unhealthy lifestyle choices (high-sodium diet, obesity, or alcohol).

Within the current healthcare industry, there have been a number of advances in the development and administration of vaccinations (Felber et al. 2014; Smith, Lipsitch, and Almond 2011). This has led to a sharp reduction in the number of cases of communicable diseases.

Overall this has had a positive outcome in under-developed counties and has reduced the number of child related deaths in poorer counties. Comparatively, there has not been as much of an improvement to reduce $PM_{2.5}$ (particulate matter mass concentration with a diameter of less than 2.5 μm) in the aerospace industry. As such, there has been a steady increase in the number of deaths each year related to $PM_{2.5}$. Between 1990 and 2015, the deaths related to $PM_{2.5}$ have increased by 20% (3.5 million to 4.2 million) (Landrigan et al. 2017). Following the current trend, by 2050 this number will rise to 6.6 million deaths per year, if nothing is done to change our current ways.

Black carbon is a key component in $PM_{2.5}$ and makes up between 0.7 $\mu g/m^3$ and 8.4 $\mu g/m^3$ (11.9% of $PM_{2.5}$ measurements by mass) (Snider et al. 2016). However, these measurements vary based on country, and relative location within cities. Air pollution is capable of traveling long distances. 11% of the black carbon pollution detected in the western United States of America was found to be produced in China (Landrigan et al. 2017). Due to the spatial variation of $PM_{2.5}$, individuals that are located closer to roadways are subject to higher concentrations of $PM_{2.5}$ composed of higher percentages of black carbon (Janssen and Weltgesundheitsorganisation 2012). This furthers the plight of impoverished individuals as it exposes them to higher levels of air pollution, increasing the likelihood of air pollution based medical complications (Landrigan et al. 2017). As was the case with climate change, the most effective method to limit the health effects of air pollution is to limit the level of pollution that is produced which can be accomplished through legislation requiring emission standards to be met.

1.3 Emissions regulation

In the interest of the public, emissions are regulated. This is done to limit the impact of climate change, and the negative impacts that pollution has on the public. These regulations

evolve over time as new methods of measurement become available. Current regulations only regulate the smoke number of an aircraft engine (SAE 2011) however, the SAE (Society of Automotive Engineers) E-31 committee has proposed a new method for emissions testing and measurements.

1.3.1 Current regulation

Current emission measurements follow the practices outlined in ARP1179 (SAE 2011). For these measurements, the smoke number (SN) is determined based on the relative reflectance of the soot collected on a reference filter. The smoke number of an engine has been correlated to the mass of black carbon emitted (Peck et al. 2013).

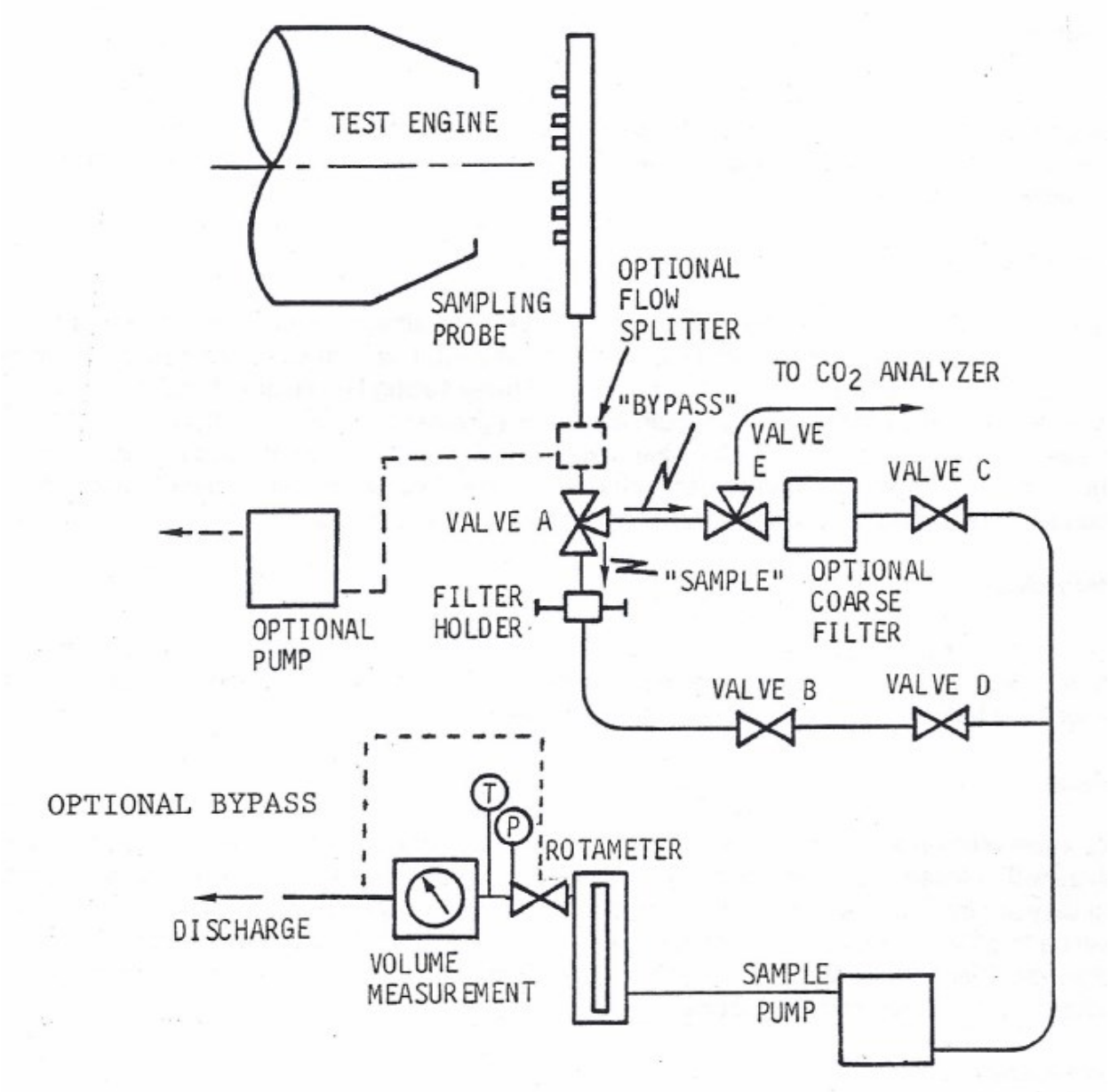

Figure 1.3: Schematic of testing for determining smoke number as outlined in ARP 1179D (SAE 2011).

A smoke number test is conducted with the setup as shown in Figure 1.3. As the exhaust sample is pulled though the system, it passes through a filter. Any particulate in the sample (BC and OC) will be collected on this filter. 50 kg of air/m^2 (mass of air per square meter of the filter area) must pass through the filter for an individual sample. Multiple samples must be taken to

ensure the accuracy of the measurements (a minimum of 3 samples within ±3 smoke number must be obtained).

After collection of the necessary sample volume, a reflectometer is used to determine the reflectance of the sample (R_s) and of a blank filter (R_w). The smoke number for the individual sample (SN') can then be calculated as,

$$SN' = 100 \left[1 - \frac{R_s}{R_w}\right] \quad [1]$$

This method of measurement and regulation is only based on the reflectance of the collected particle mater. Larger particles scatter and absorb more light (Magi et al. 2005) causing them to have a larger impact on the smoke number measurements. As such, an engine that produces a large number of small particles has the potential to have the same smoke number as one that produces a small number of large particles. As was previously stated, the small particles (specifically $PM_{2.5}$) have a large impact on both climate change and public health. To better regulate these devices and better capture the number of particles produced, new regulations are required.

1.3.2 Future regulation

The European Union is paving the way with future emission regulations in the automotive sector. As of 2011 emissions from heavy-duty and personal vehicles are measured by both the mass of the emissions, and the particle count. These measurements are conducted using a filter based method to determine the mass of emissions and a CPC for particle counts (European Comission 2011). This is a change in measurement that will eventually occur within the aerospace industry.

While the automotive industry has an adequate solution to collect samples for emission requirements, the same methods cannot be used within the aerospace industry. Aircraft engines have a much higher cost to run as compared to automotive engines. As such, collecting samples on filters is not an ideal method to determine the mass of particulate produced per kg of fuel burned; to collect enough mass on a filter such that accurate measurements can be obtained will cost far too much.

The SAE E-31 committee recently drafted an Aerospace Recommended Practice (ARP) document for the measurement of aircraft engine non-volatile particulate mass and number. A schematic of the proposed setup can be found in Figure 1.4. The system is composed of 3 sections, the collection section (region where sample inlets are to obtain particulate across the profile of the exhaust), the transfer and conditioning section (region where sample is diluted and large particles (those greater than 1μm in diameter) are removed) and the measurement section (region where particle count and particle mass are measured). To determine the dilution factor, the CO_2 concentration is measured at various stages. In addition to this, pressure and temperature measurements are made such that the standard flow rate at each stage of the system can be determined. These measurements are made both in the transfer section and the measurement section. This ensures the measurements are accurate to the sampling end of the setup.

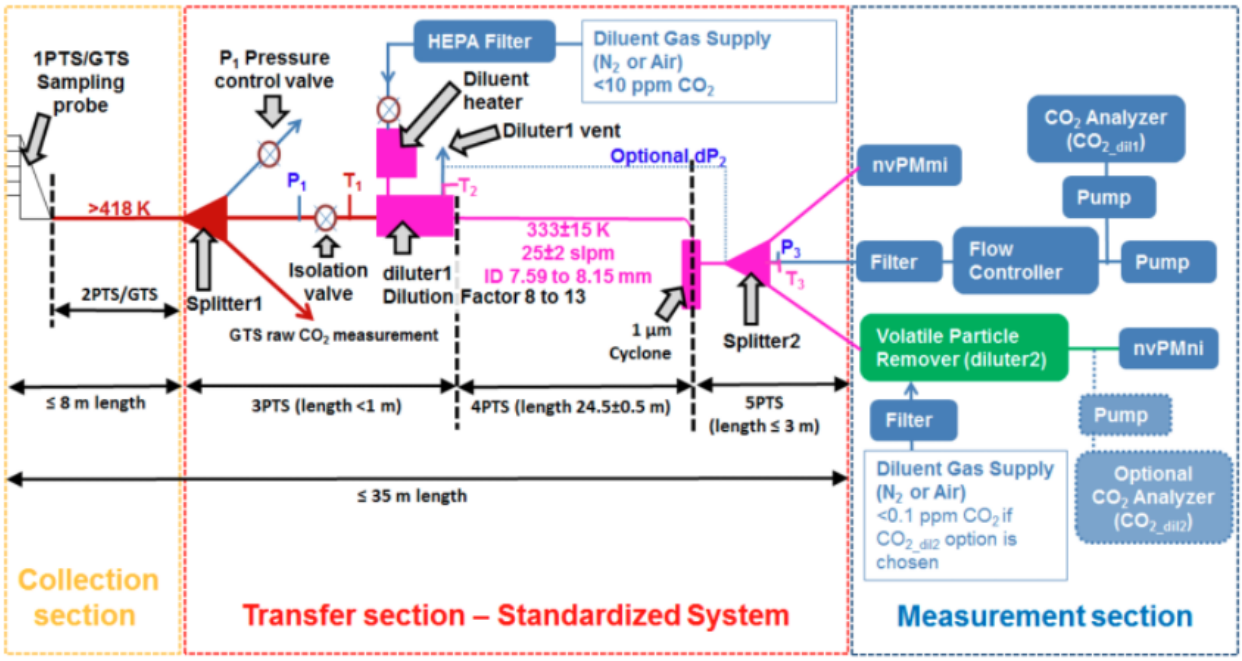

Figure 1.4: Schematic of proposed testing apparatus from SAE E-31 (SAE 2013).

Within the measurement section two measurement devices are used; they are a non-volatile particulate matter mass instrument (nvPMmi) and the non-volatile particulate matter number instrument (nvPMni). A condensation particle counter (CPC) would operate as the number instrument. A CPC operates by condensing butanol vapour onto the inlet sample (particles act as preferred nucleation sites for condensation to prevent butanol particles from forming) (Cheng 2011). The diameter of the particles rapidly increases and are passed through an optical detector that then counts them. Flow through the system is regulated using a vacuum pump and a critical orifice. This ensures the flow through the system is constant and known such that the particle concentration can be determined from the particle count. A schematic of how the CPC operates can be seen in Figure 1.5.

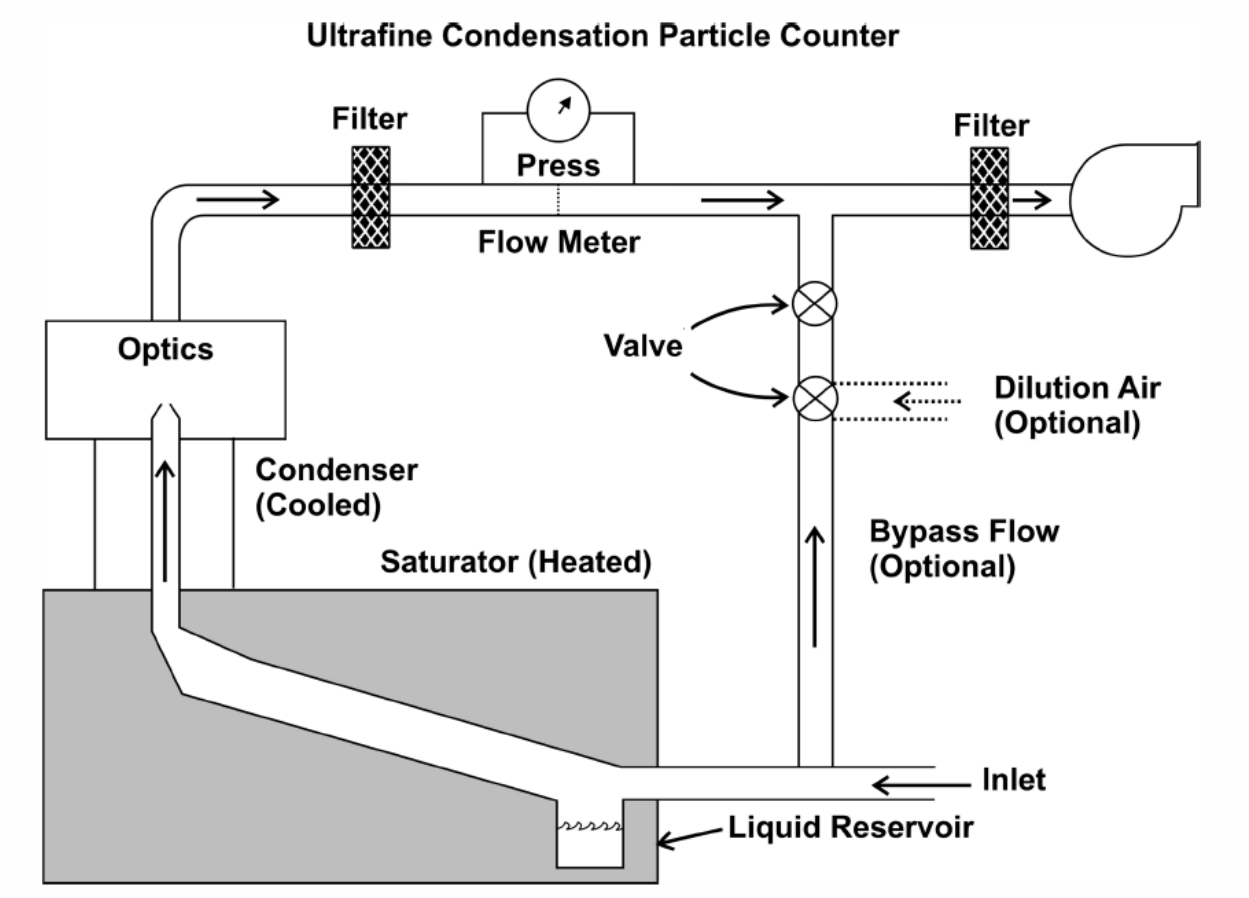

Figure 1.5: Schematic of conductive cooling CPC (TSI 3022 CPC) (Cheng 2011)

For the particulate mass instrument (nvPMmi) two real-time devices that could be used are the laser-induced incandescence instrument (LII) (particles in this device are heated with a laser and the radiative emissions are measured, this allows the volume fraction of the particles to be determined (Schulz et al. 2006) and the photo-acoustic Micro-Soot Sensor (MSS) (particles in this device are heated with a pulsed laser and the resulting pressure wave is amplified in a resonance chamber and then measured (Schindler et al. 2004). Both of these devices are capable of giving a real-time measurement of an aerosol mass concentration. However, they are both affected by the local temperature and pressure. To correct for this, they actively measure both properties internally. Furthermore, the device measurements will drift from zero. As such, the devices must be recalibrated at each testing location to provide accurate measurements.

1.4 Calibration of measurement devices

The SAE recommended practice includes provisions that these instruments should be calibrated before use in engine testing. For particulate mass, the SAE E-31 committee has recommended that filter sampling with carbon burn-off (elemental carbon/organic carbon (EC/OC) analysis following the NIOSH 5040 protocol) be used as a calibration standard for non-volatile particle mass. However, there are a number of different calibration techniques that can be used.

1.4.1 Current calibration methods

NIOSH 5100 defines an accepted method for calibration. This method relies on the change in mass of various filters used to capture black carbon, which is then weighed and compared to the mass of the filter before testing procedures began. A measurement is conducted by measuring the initial mass of a filter on an appropriate scale (this is selected for based on the resolution of measurements that are desired). The aerosol is then passed through the filter and a challenge instrument (a device that is being calibrated), and the particulate matter that is present will be collected on the filter while concentration measurements are taken on the challenge device simultaneously. This collection is done a measured period of time (the length of time is selected for based on the expected mass concentration of the aerosol, and the flow rate of the aerosol). The change in mass of the filter must be large enough that the uncertainty in the initial measurements of the filter mass is negligible. For measurements where small concentrations of particles are used, it can take hours or days to collect enough sample. A second measurement of the filter is then taken, and the actual mass concentration can be calculated and compared to measurements that were taken on the challenge instrument.

Gravimetric assays uncertainty is based around the number of samples collected, as well as the properties of the particles used. As such, the uncertainty can be limited by making repeat measurements. While this is advantageous, it greatly increases the length of one calibration. This is made even longer by the extreme length a single measurement can take. As such, gravimetric methods of calibration will not work for the proposed calibration standard as the cost of calibration would be far too much.

As the SAE E-31 committee has recommended, the proposed method of calibration for future emission regulations is using NIOSH 5040. The procedure for NIOSH 5040 is similar to that of NIOSH 5100 in that the aerosol is passed through a filter and challenge instruments in parallel, and the particulate is collected on the filter while active measurements are taken on the challenge instrument. The time of collection is again recorded as well as the sample flow rate. The aerosol used for these tests must be a carbon particle source (a commonly used source is an inverted co-flow burner as suggested by Stipe et al. (2005). The filter sample collected is then placed in a thermal-optical analyzer, where the mass of EC and OC are both measured. Within the thermal-optical analyzer, the sample is first heated in an oxygen-free environment (Bae et al. 2004). This allows OC to be converted to carbon dioxide, which is then passed through a methanator and converted to methane. The quantity of methane is then measured using a flame ionization detector. Once all of the OC has reacted, the test chamber is reset and is filled with a new gas mixture that includes oxygen. The same process is then repeated, however, it is now the remaining EC that is oxidized. This allows both the EC and OC to be quantified independently such that devices that measure only one of these or both of these forms of carbon can be calibrated.

NIOSH 5040 is a very time consuming procedure and is not suitable for engine cell calibration as samples need to be sent to a lab for analysis. Multiple samples must be collected to linearly calibrate an instrument. One calibration can take weeks to complete as enough sample must be collected on each filter to be accurately measured. The process is also highly variable, having a reported repeatability (expressed as one standard deviation) of 8.5% at a concentration of 23 μg/m3 (NIOSH, 2003). It is noted that this repeatability is not an estimate of the total uncertainty of the technique but rather it is only an expression of the consistency of the technique using the same instrument.

1.4.2 Proposed method of calibration

The current methods of calibration are both labour intensive, and take a large amount of time. As an alternative, Symonds et al. (2013) has suggested a CPMA (Centrifugal Particle Mass Analyser)-electrometer setup to be an alternative method to measure aerosol mass concentrations for calibration purposes. This method is capable of providing real time measurements of aerosol concentration, allowing for equipment calibrations in a much shorter period of time. This system works through the use of the mass to charge ratio of the calibration aerosol. A calibration system of this nature is composed of 4 key pieces of equipment: an aerosol source, an aerosol charger, a mass classification device (such as the CPMA or an Aerosol Particle Mass Analyser (APM) and a Faraday cup-electrometer system (this can be either two separate pieces of equipment or a single enclosed system such as the TSI aerosol electrometer). Figure 1.6 displays the general schematic for a system as proposed by Symonds et al (2013).

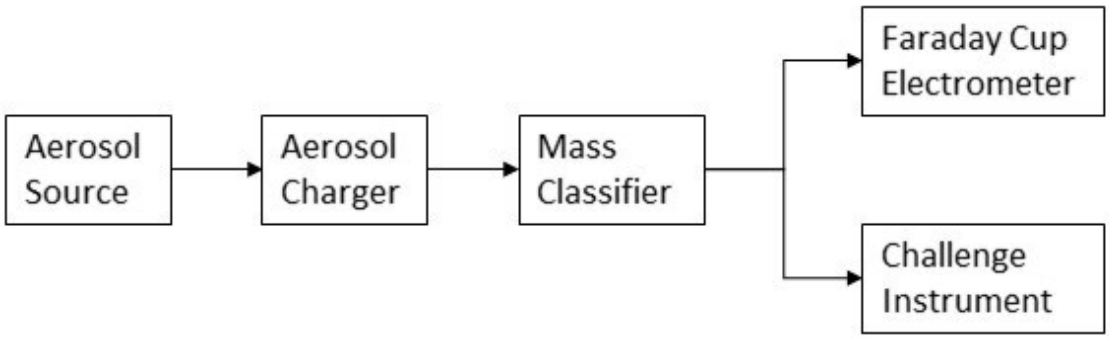

Figure 1.6: Schematic of calibration system using mass to charge ratio for classifying the aerosol.

Symonds et al proposed the use of the CPMA as the mass classification device in the system. The CPMA selects for particles based on their mass to charge ratio (Olfert and Collings 2005). This device consists of two concentric drums that rotate at slightly different speeds (the ratio of outer angular speed to inner angular speed is typically 0.9696 (Cambustion 2011). As the drums rotate, particles in the gap between the drums are forced out by a centrifugal force. To counteract this, a voltage difference is applied between the drums creating an electrostatic force that pulls positively charged particles towards the inner drum. Thus, particles with a specific mass to charge ratio will be selected and pass through the device. Figure 1.7 displays the effects of the centrifugal force and electrostatic force that are present as particles pass through the device. The APM operates in a similar manner as the CPMA, however, the speed ratio of the device is 1, *i.e*. the angular velocity is the same between both the inner and outer drums.

.

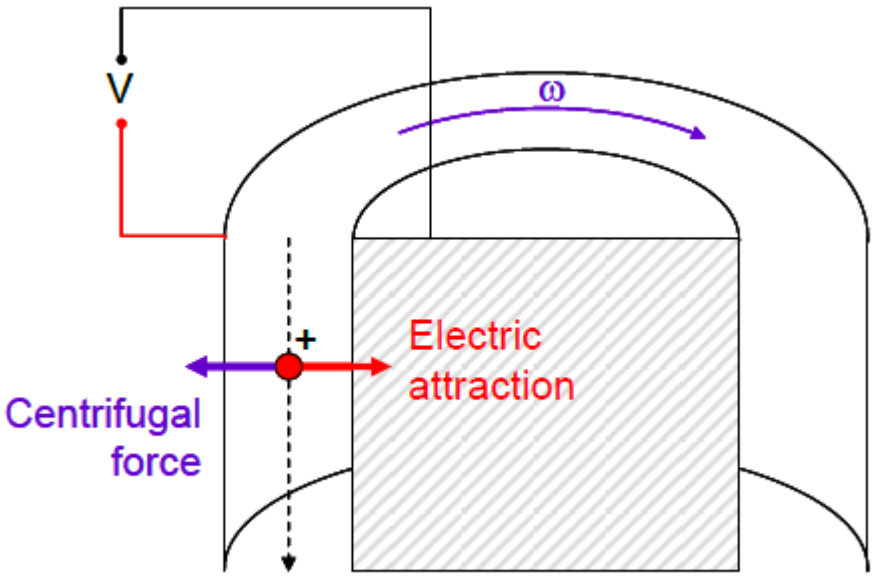

Figure 1.7: General schematic of CPMA. (Cambustion 2011)

For classification these devices require the aerosol to be electrically charged. There are a number of different methods to achieve this. Three such examples are displayed and summarized in Figure 1.8. Each charger has advantages and disadvantages in regards to the transmissibility (the ratio of particles that make it through the device to the number of particles that enter) and the level of charging (Dhaniyala et al. 2011). The three methods of charging presented are all corona chargers (a method of charging that utilizes current flow from an electrode to ionize a flowing gas producing a plasma, i.e. the particles within the gas have become charged by either adding or removing electrons though the use of a strong electric field). This method of charging has an advantage as it imparts a very high level of charge on the aerosol; as such, the CPMA-electrometer system will have few uncharged particles that pass though (Symonds, Reavell, and Olfert 2013).

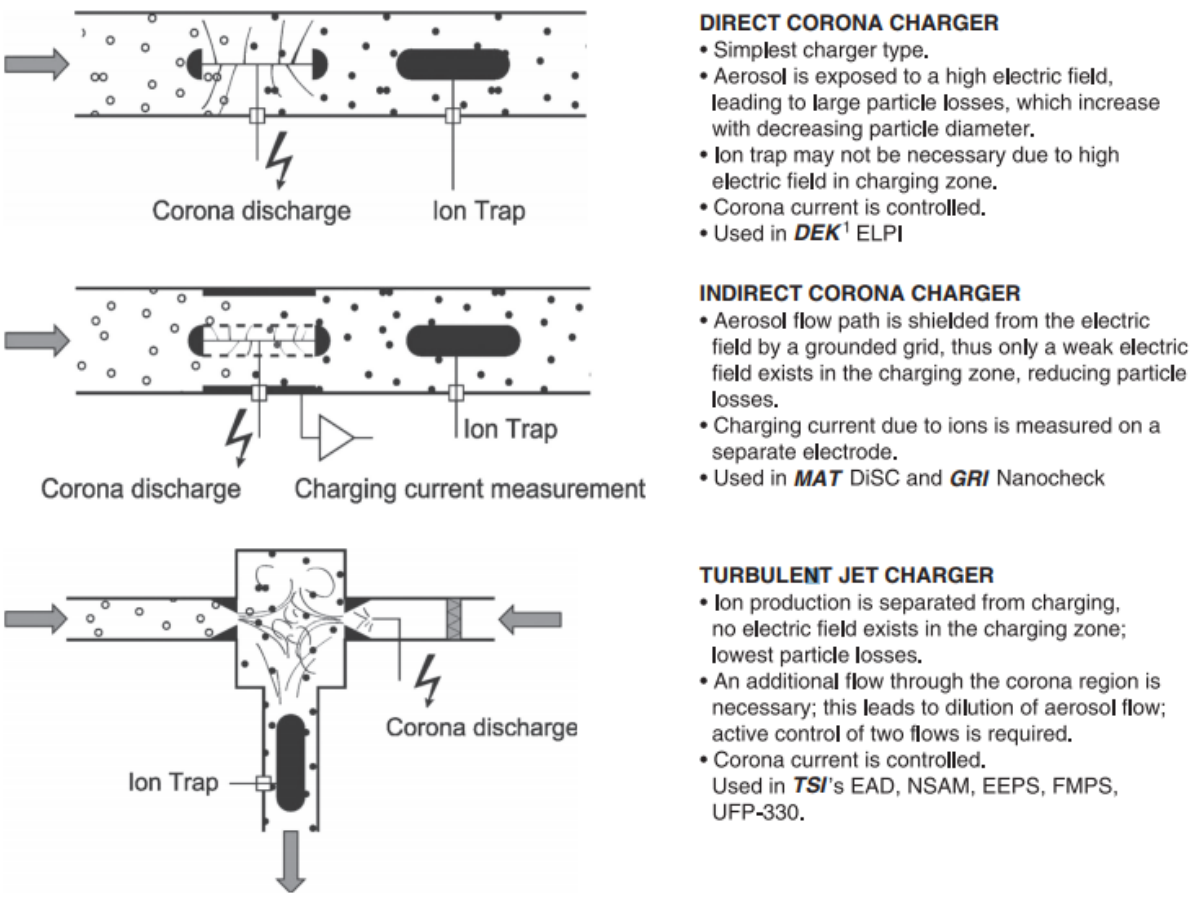

Figure 1.8: Three examples of aerosol chargers (Dhaniyala et al. 2011).

Limiting the number of uncharged particles is important for calibration purposes as the challenge instrument will measure these uncharged particles, while the electrometer will not. The total mass concentration passing though the CPMA can be calculated as follows (Symonds, Reavell, and Olfert 2013).

$$m_{\text{total}} = m_0 + M_{+1}(n_{+1} + 2n_{+2} + 3n_{+3} + \cdots) \qquad [2]$$

where m_0 is the mass of uncharged particles, M_{+1} is the mass set point of the CPMA (the mass of a particle that has one charge on it) and n_i is the number of particles with i charges. The

equation determines the total mass that has passed through the system, m_{total}. Similarly, the current flow, I, measured by the electrometer is:

$$I = Qe(n_{+1} + 2n_{+2} + 3n_{+3} + \cdots) \quad [3]$$

where Q is the volume flow rate and e is the elementary charge (1.602 x 10^{-19} C). Equations 2 and 3 can be combined to give the following:

$$m_{\text{total}} = m_0 + \frac{M_{+1}I}{Qe} \quad [4]$$

The total mass though the system includes all charged particles (where particles with 2 charges have twice as much mass as those with one) and all uncharged particles. However, though the use of a corona charger and high speeds of the CPMA, the number of uncharged particles can be limited such that they will have a negligible effect on the measurement (Symonds, Reavell, and Olfert 2013).

The charged particles passing through the system is measured using a combination of a Faraday cup to capture the charge of the aerosol and an electrometer to measure the electrical current. A Faraday cup consists of two metal cups, the smaller of which sits inside the larger, but is electrically insulated from the first via low conductance seals (as seen in Figure 1.9) (Dhaniyala et al. 2011). This allows the inner cup to be completely electrically insulated from the external environment while still interacting with the aerosol. The inner cup has a mesh filter that is used to capture the charge from the aerosol, and thus a voltage potential develops between the two cups and an induced current between the plates can be measured by the electrometer. The

electrometer connects the two cups in the Faraday cup with a low noise BNC cable to limit the amount of interference or noise present in the measurement (while it is possible to use a regular BNC cable it is not ideal as fluctuations due to noise can be large relative to the measured current).

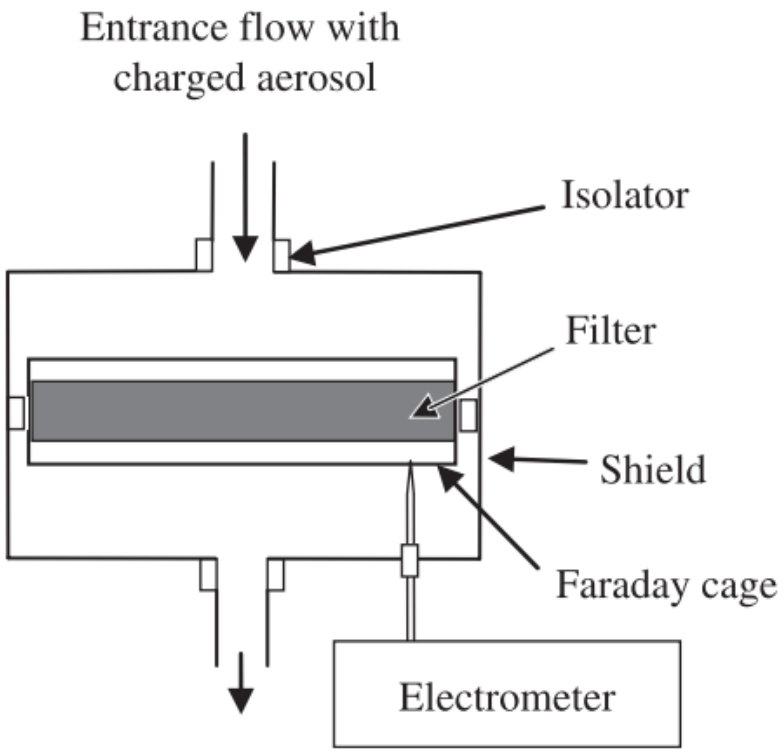

Figure 1.9: Schematic of Faraday Cup. (Dhaniyala et al. 2011)

The CPMA-electrometer system is capable of measuring low aerosol concentrations; the limiting factor to these measurements is the sensitivity/insulation of the faraday cup, and the lower detection limit of the electrometer. Manufacturing a better insulated device will prevent any current leakage and better capture the true current passing through the system and thus the measurements will be more accurate (Högström et al. 2014). Similarly, having a higher amount

of charge on the particles increases the current flow which will allow for lower aerosol concentrations to be measured.

The SAE E-31 committee would like a system that could be deployed to engine manufacturer test facilities and used to verify instrument calibration before engine tests. Such a device must be compact enough such that it can be easily shipped, while still providing all the necessary equipment to conduct the calibration. As the device is intended to be shipped from location to location it is required to be rugged.

1.4.3 Uncertainty of CPMA-Electrometer system

The CPMA-electrometer system has a number of pieces of equipment that are necessary to collect measurements. Equation 4 displays the calculation required for the total mass concentration. This value is based on Q, the volume flow rate, M_{+1}, the mass set point of the CPMA, I, the current measurement from the Faraday-cup electrometer system, m_0, the mass of uncharged particles and, e, an elementary charge. Within this system it is assumed that all particles are charged, and thus the uncharged mass is zero. In addition to this, the elementary charge has been previously well defined and it can be assumed the uncertainty in this value is negligible. As such, the uncertainty of the overall CPMA-electrometer system is based only on the uncertainty of the volume flow rate, the mass set point, and the measured current.

Högström et al. (2014) have examined 8 separate Faraday cup-electrometer systems for measuring charged particles up to 200 nm in diameter. The 8 devices were tested simultaneously by splitting the aerosol flow such that each system received a similar sample. A number of measurements were taken, at various concentrations and particle sizes. Before and after each test, zero measurements were taken to account for any drift caused by variations due to temperature

or pressure changes in the environment. Overall, when the measured diameter was between 6 nm and 20 nm, the devices were within ±5%, however, some of the tested devices were much closer to the expected measurement with one of them being closer than ±1%. With such a high level of variation between devices, it is likely different designs of Faraday cup-electrometers will have different levels of variation, with an expected upper limit of roughly ±5%.

The purpose of the work reported here was to experimentally determine the repeatability and intermediate precision of a CPMA-electrometer system. Previously, the CPMA-electrometer system was estimated to have a standard uncertainty of only 4.3%. The standard uncertainty is an estimate of the total uncertainty (coverage factor, k=1), however, the value was based on theoretical estimates on the uncertainties in the flow meter, electrometer, and CPMA. In this study, an attempt is made to quantify these theoretical estimates through experimental measurement as part of developing a robust demonstration of the capacity and uncertainty of the CPMA-electrometer calibration method.

For the purposes of testing procedures, the definition for repeatability and intermediate precision are those found in the International Vocabulary of Metrology, 3rd edition. As such, repeatability measurements were taken, ensuring the same measurement procedure, same measuring system, same operating conditions, same location, using similar particles for each test. Tests for repeatability measurements were collected over a short period of time to ensure none of these conditions changed. Similarly, “intermediate precision” measurements were conducted using different measuring systems with replicate measurements being taken on similar particles that were used for testing, on each system.

Intermediate precision measurements were conducted following the procedure found in ISO 5725-3. For each measurement, where possible, either the time interval, the

equipment, the operator or the calibration was varied. For the purposes of the definition, a short period of time is defined as one day. Within this document, the intermediate precision can be defined as M=1, 2, 3, or 4, where M is the number of variables that are different. For this study, only the time interval or the equipment was varied, thus M only has the possible values of 0, 1 or 2. The intermediate precision is the standard deviation, of all of the data that falls into a group of data, e.g. the time-different intermediate precision of a device can be found by calculating the standard deviation of all data collected on the same device, over a period of time. As such, this intermediate precision will be the M=1 intermediate precision. The repeatability (as previously defined) of a device can be found by calculating the intermediate precision of M=0. The reproducibility of the device displays the maximum variance that can be expected by using the device (i.e. intermediate precision of M=4). The bias of a device is the difference between the mean of several measurements and the value of the accepted standard.

1.5 Overview of thesis

This thesis is composed of 4 chapters. Chapter 2 discusses the components of the CPMA-electrometer setup and all other equipment used to determine the intermediate precision of the components of the CPMA-electrometer system. Chapter 3 covers the experimental procedures that were used to test the CPMA, Chapter 4 covers the testing procedures to test each other piece of equipment, (both chapter 3 and 4 also include the results from said experiments and calculations for the intermediate precision of the system as a whole). Chapter 5 presents a summary of the results discussed, and any improvements that could be made through future work.

Chapter 2 Description of Equipment

The CPMA-electrometer system requires multiple pieces of equipment to operate. A general schematic of the testing apparatus for the CPMA-electrometer system used to calibrate black carbon instruments can be seen in Figure 2.1. The main components of the system used are: inverted burner, catalytic stripper, Cambustion Unipolar Diffusion Aerosol Charger (UDAC), Cambustion Centrifugal Particle Mass Analyzer (CPMA), static mixer, Faraday cup, Keithly electrometer, pump and flowmeter. A challenge instrument is placed downstream of the static mixer in parallel with the particle current measurement. This allows the CPMA-electrometer system to measure the current flow rate as the challenge instrument measures the black carbon mass concentration ($\mu g/m^3$). Using the current flow rate from the electrometer, the mass set-point of the CPMA and the volume flow rate as set by the flow controller, the mass concentration can be calculated. The mass concentration can be compared between the two systems. The main components of the CPMA-electrometer system can be categorized into four categories: particle generation, conditioning, classification, and measurement.

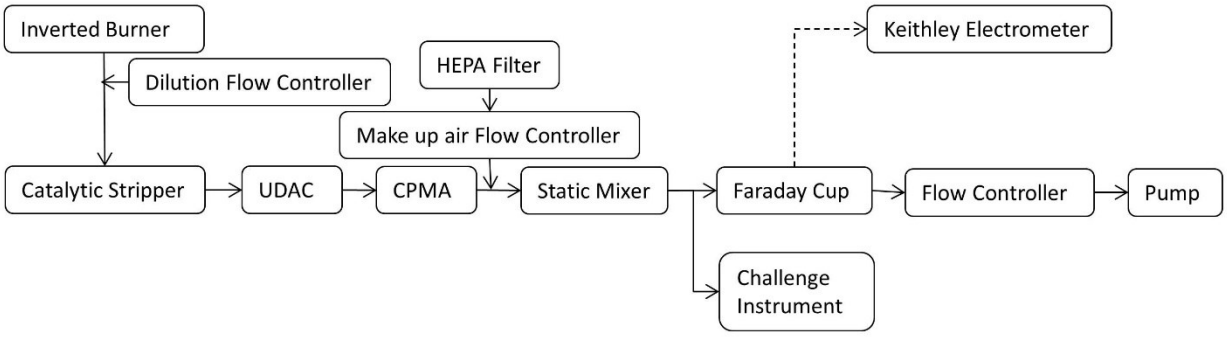

Figure 2.1: CPMA-electrometer system schematic.

The overall CPMA-electrometer system was tested as presented in Figure 2.1. This system has the same components as proposed by Symonds (2013). The repeatability and reproducibility of the system was tested with experiments of the whole system. In addition to these tests the individual components of the CPMA-electrometer were tested for each device's repeatability and reproducibility. Generally, the schematic for each test was similar to the one presented in Figure 2.1, however, the testing of some components used different equipment in their respective experiments. The full CPMA-electrometer setup and the components of this system will be described in this chapter. Any differences for the testing of the individual components will be described in the next chapter when each experiments setup is presented.

2.1 Equipment of CPMA-electrometer system

As was discussed in chapter 1, the CPMA-electrometer system has 5 key components. These include the aerosol source, aerosol charger, a mass classification device (CPMA), the Faraday Cup-electrometer and a challenge instrument. Each of these components will be discussed in relation to what device was used for each step.

2.1.1 Aerosol generation

Particles were generated using a methane co-flow inverted diffusion-flame burner. The components included in particle generation include the inverted burner and all of its related flow controllers. It has been previously shown that an inverted burner produces a stable flame, with a highly stable black carbon size distribution (Stipe et al, 2005). The inverted burner used had 1.48 SLPM of methane, 17.2 SLPM of combustion air, and 200 SLPM of dilution air. The standard temperature and pressure were 0 °C and 1 atm, respectively. This provided a high particle concentration that had a large range of particles with variable effective diameters and masses. A second flow controller, the dilution flow controller, allowed for secondary dilution to occur in

the sample line. This provided a method to vary the concentration of the aerosol in the measurement system.

One item of concern when using an inverted burner is the warm up period. While inverted burners are visibly stable, there is an initial warm up period in which the particle distribution varies. To avoid any artifacts in the measurement due to the warm up, the inverted burner was provided at least 1 hour to warm up, prior to conducting tests.

2.1.2 Aerosol Conditioning

In order to properly condition the particles for testing, two pieces of equipment were used: the catalytic stripper (Catalytic Instruments, 25 L/min capacity), and the unipolar diffusion aerosol charger (UDAC; Cambustion Ltd.). The catalytic stripper, composed of a heating unit surrounding a catalytic substrate, was intended to evaporate and catalyze any volatile material that remained on the non-volatile particles. As such, all particles exiting the stripper were composed of only non-volatile material and it is assumed this material is black carbon (Petzold et al, 2013).

The second component, the UDAC, is designed to provide a unipolar electric charge to the black carbon particles in the aerosol. Figure 2.2 displays a schematic of the charging core within the UDAC. The central component of the UDAC is a fine corona wire charging unit that creates highly mobile ions (Cambustion 2012). These ions interact with the aerosol, imparting their charge on the particles. The charging current in this unit is controlled via the corona voltage that is applied to the unit. As such, the net ions in the aerosol flow can be controlled, giving an adjustable charge to the aerosol. This method of charging generates an aerosol where individual particles can have anywhere from zero to multiple charges on it. However, by setting the device

charging ion current to a higher value, the number of charges is higher, and the number of particles with no charges are reduced (Biskos, Reavell, and Collings 2005).

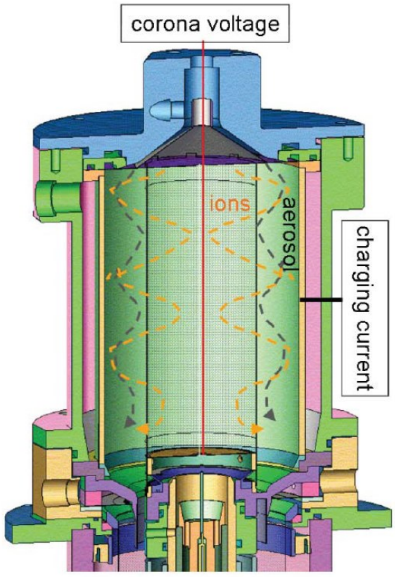

Figure 2.2: Charging core schematic for Cambustion UDAC (Cambustion 2013).

2.1.3 Classification

Classification was conducted using the CPMA (Cambustion Ltd.; Olfert et al, 2005). This device selects particles based on the mass to charge ratio of the charged particles. As was discussed in Chapter 1, the CPMA consists of two rotating cylinders, with the inner cylinder rotating faster than the outer, and a voltage difference between the two cylinders. As such, the centripetal force pushes particles out, with a force that varies with mass, and the voltage difference pulls charged particles in with a force that varies with the charge. This allows for a specific mass to charge ratio to be selected by changing the speed of the cylinders, and the voltage difference between them. This makes the CPMA unique as the properties required for

selection, mass and charge, can be selected using traceable methods. A cut-out view of the CPMA is shown in Figure 2.3. A detailed analysis of the theory behind the CPMA is presented in Chapter 3.

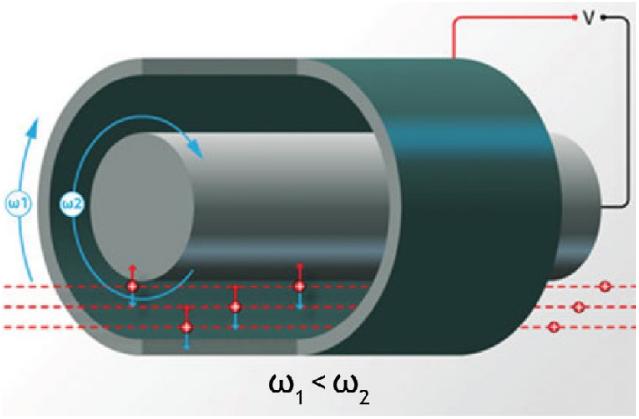

Figure 2.3: CPMA classification schematic. The red arrows represent the electric force, while the blue arrows represent the centripetal force (Cambustion 2011).

2.1.4 Particle Charge Measurement

Mass concentration measurement by the CPMA-electrometer system is accomplished by measuring the current of the particles, the mass flow rate of the aerosol, and the mass to charge ratio of the classified particles. The current measurement is accomplished with the Faraday cup connected to a Keithley electrometer (Keithley 6517B and Keithley 6514). The mass flow rate of the aerosol is controlled and measured by a mass flow controller (Alicat MC-5SLPM-D and Aalborc GFC37) while the mass to charge ratio of the particles is set by the CPMA as described above. To generate flow through the system, a vacuum pump induces a low pressure environment downstream of the flow controller. The flow controller is set to allow 4.0 standard L/min (SLPM; referenced to 0˚C and 1 atm) though the device, producing a fluid flow of 4.0

SLPM though the system. This flow travels though all devices described thus far, including the UDAC, CPMA and the Faraday cup.

The Faraday cup consists of two metal cups, the smaller of which sits inside the larger, but is electrically insulated from the first via low conductance Teflon seals (as seen in Figure 1.9). This allows the inner cup to be completely electrically insulated from the external environment while still interacting with the aerosol. The inner cup has a mesh filter that is used to capture the charge from the aerosol, and thus a voltage potential develops between the two cups and an induced current between the plates can be measured by the Keithley electrometer. The electrometer connects the two cups in the Faraday cup with a low noise BNC cable.

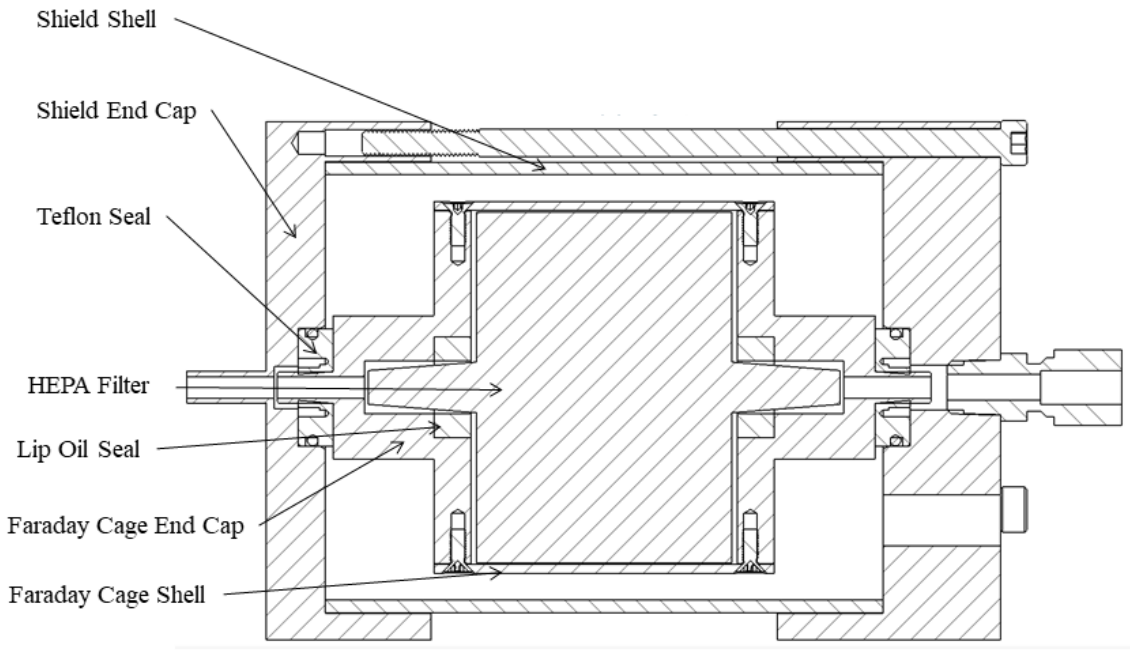

Figure 2.4: Cutout view of Faraday Cup used.

By measuring the current of the aerosol, at a set flow rate of 4.0 SLPM, and knowing the mass set point of the CPMA, the mass concentration of the aerosol, M_∞, can be found;

$$M_\infty = \frac{I\, M_{+1}}{Q} \qquad [5]$$

where I is the measured current, M_{+1} is the mass to charge ratio (set point of the CPMA), and Q is the flow rate of the fluid. Since each of these values can be measured using first order traceability methods, the CPMA-electrometer can measure the mass of an aerosol with first order methods, an essential property of calibration systems.

2.1.5 Other Aerosol Conditioning Elements

Two other elements of the system have not been described in the above four categories. These are the HEPA filter, and the static mixer. Both of these items are used after classification has occurred, but before any measurements have been done. The HEPA filter, in conjunction with the make-up air flow meter, is used to provide particle-free makeup air to the system. This is necessary as the CPMA has a maximum suggested flow rate of 4 LPM which is generally lower than the desired flow rate through the Faraday cup and the instrument to be calibrated. Since the Faraday cup captures the charge from the aerosol, having move aerosol pass though the Faraday cup will give a larger reading and thus improve the sensitivity of the device. This can be done by setting the flow rate though the Faraday cup to a higher value.

To achieve the desired total flow rate, HEPA filter make-up air is combined with the classified aerosol, thus lowering the concentration, but maintaining the mass to charge size classification. The reason for the 4 LPM upper limit of the flow rate though the CPMA is that

flow rate impacts the resolution of the transfer function (i.e. the range of particle mass to charges that make it through the device). The static mixer serves to ensure that the classified aerosol mixes well with the HEPA filtered air before it reaches the electrometer and calibration instrument.

Two systems were used for the repeatability and intermediate precision measurements. Table 2.1 displays a summary of each of the components. Some components were used in both systems (such as the catalytic stripper) while the key components of the systems had duplicates (UDAC, CPMA, Electrometer). Two separate faraday cups were used. Both were made in-house and as such do not have a part or serial number.

2.2 Conclusion

The CPMA-electrometer system has a number of components that the final measurements rely on. To determine the repeatability and intermediate precision of the overall system, each component must be understood. The following two chapters will examine the various components of the system to determine these values. Since the CPMA is such an integral component of this system, and there has been limited analysis on it in the past, Chapter 3 will be dedicated to understanding this device. Chapter 4 will examine the rest of the components of the CPMA-electrometer system and the system as a whole.

Table 2.1: List of components for each of the two CPMA-electrometer systems and the equipment used for the tandem CPMA test. UofA stands for the University of Alberta while NRC stands for the National Research Council of Canada.

Component	Provider	Manufacturer	Part Number	Serial Number
Catalytic Stripper	NRC			
UDAC B	UofA	Cambustion		U112
UDAC A	NRC	Cambustion		U111

CPMA B	UofA	Cambustion		C313
CPMA A	NRC	Cambustion		C220
AFM B	UofA	Cambustion		F113
AFM A	NRC	Cambustion		F111
Electrometer B	UofA	Keithley	6517B	1384954
Electrometer A	NRC	Keithley	6514	4012969
Flow Controller B	UofA	Alicat	MC-5SLPM-D	119158
Flow Controller A	NRC	Aalborc	GFC37	364572-1
Pump B	UofA	Thomas	G24 Series	
Pump A	NRC	Gast	1532	
CPC	UofA	TSI		3776
Atomizer	UofA	TSI		3076
Diluter	UofA	Dekati		DI-1000
DMA	UofA	TSI		3081

Chapter 3 Tandem CPMA-CPMA testing

The CPMA is the integral component of the CPMA-electrometer measurement system. As such, understanding limitations of the CPMA is necessary to determine the uncertainty of the overall system. This chapter analyzes the CPMA and determines the overall repeatability and reproducibility of it.

3.1 Background on particle mass classifiers

Particle mass analyzers, such as the centrifugal particle mass analyzer (CPMA) and the aerosol particle mass analyzer (APM), have allowed for numerous new avenues of aerosol research to be explored as classification is based on the mass to charge ratio of the particles. Particle mass analyzers operate by passing charged particles between two rotating cylinders with a potential difference between them. This generates two forces on each particle; a centrifugal force and an electrostatic force. These forces are based on the number of electric charges and the mass of the particle for a given rotational speed and electrical potential between the cylinders of the analyzer. As such, particles with a narrow range of mass to charge ratio (sometimes called 'specific mass') will pass through the device. Sometimes the electrical charge state of the particles is unknown (or can be inferred), so that the mass of the particles is known.

Although the focus of this thesis is to use the CPMA for instrument calibration, the CPMA is also used in many other applications which are briefly mentioned here. One common application of the CPMA is to use it in conjunction with a differential mobility analyzer (DMA) and condensation particle counter (CPC) to determine the relationship between the mass and mobility of the particles (McMurry et al. 2002). In this system, typically, particles are first selected based on their electric mobility as they pass through the DMA. A mass to charge

distribution of the narrow band of selected particles can be found by stepping the CPMA through a range of setpoints (by changing the voltage and/or rotational speed) and measuring number concentration of the CPMA-classified particles with a CPC. The mass-mobility relationship can be used to determine the effective density of the particles, defined as the mass of the particle divided by its mobility-equivalent volume, or to calculate the mass distribution of an aerosol from the count distribution (Park, Kittelson, and McMurry 2003). Rawat et al. (2016) have extended this technique to calculate a two-variable distribution function by data inversion, which shows the count or mass distribution of the aerosol as a function of size *and* mass. The mass-mobility relationship can also be used to determine the dynamic shape factor of particles (DeCarlo et al. 2004) or to estimate the size the primary particles in aggregates (Dastanpour et al. 2016; Eggersdorfer et al. 2012).

The addition of a thermodenuder between the DMA and the CPMA provides insight into the distribution of volatile material in the aerosol. The mass fraction of volatile material on a particle can be measured by measuring the total mass of the DMA-classified particles (undenuded) with the CPMA, then measuring the non-volatile mass of the particles by denuding the particles before measurement with the CPMA (Sakurai et al. 2003). By measuring the fraction of purely volatile particles (using a DMA-thermodenuder-CPC system), with knowledge of the volatile mass fraction, allows for the determination of the aerosol mixing state and the mass distributions of non-volatile particles, surface-condensed volatile material, and pure volatile particles (Dickau et al. 2016).

As discussed in the previous chapters of this thesis, the CPMA has also been used in a method of calibrating mass concentration instruments. In this method, particles are charged using a unipolar diffusion aerosol charger then classified with the CPMA to produce an aerosol

with particles of a specific mass to charge ratio. The flow is then split between a faraday cup-electrometer system and a challenge instrument (Symonds, Reavell, and Olfert 2013). The current measured by the electrometer, the flow rate, and CPMA set point are used to calculate the mass concentration of the aerosol which is used to calibrate the challenge instrument. (Dickau et al. 2015) have previously used a CPMA-electrometer system to calibrate a laser-induced incandescence instrument (LII 300) and a photo-acoustic micro-soot sensor with high levels of correlation (>0.99 R^2).

In the applications above, it is useful to know the transfer function of the CPMA. The transfer function is a relationship describing the fraction of particles that pass through the device as a function of the operating conditions and the particle mass to charge ratio. The theoretical transfer function of the CPMA has been modelled by Olfert and Collings (2005), who created models which include or exclude the effects of particle diffusion in the classifier. While the theoretical transfer function of the device can be calculated, there have been limited data collected on how the actual transfer function of the device deviates from the theoretical model (Olfert et al. 2006), and there are no data available for the commercially available CPMA from Cambustion Ltd.

Previously, many studies have used two DMAs in series ('tandem DMAs') to study the transfer function of the DMA (Birmili et al. 1997; Stratmann et al. 1997; Martinsson, Karlsson, and Frank 2001; Li, Li, and Chen 2006; Collins et al. 2004). In these studies, the upstream DMA was set such that a narrow particle distribution was allowed to pass through the first DMA and the total number concentration is measured, the downstream DMA voltage was then stepped or scanned across the expected distribution and the downstream number concentration measured. The distribution of particle counts (particle concentration vs. DMA

voltage) exiting the second DMA is a result of the convolution of the two DMA transfer functions. De-convolution or data fitting routines are used to calculate the actual transfer function (Li, Li, and Chen 2006) or how the actual transfer function differs from an ideal case (Birmili et al. 1997; Stratmann et al. 1997; Collins et al. 2004), assuming that the two DMAs have identical transfer functions. Martinsson, Karlsson, and Frank (2001) extended this methodology using three separate DMAs and repeating multiple tandem DMA experiments with different combinations of DMAs in order to determine differences in the transfer functions between the DMAs.

In this study, we use a tandem CPMA methodology to quantify non-idealities in the actual transfer function of the CPMA. Tandem CPMA experiments are used to measure a particle loss parameter (*e.g.* due to impaction or diffusion losses in the instruments), a transfer function broadening parameter (*e.g.* due to diffusional broadening or other effects), and the offset in the mass setpoints (e.g. due to differences in voltage or speed calibration, or geometry). These parameters can be used to correct the ideal transfer function so that CPMA data analysis routines (*e.g.* inversion) can be improved. In the specific application of the CPMA-electrometer calibration system, the offset parameter provides describes the reproducibility of the CPMA.

3.2 Method

To test the properties of the CPMA a tandem CPMA-CPMA setup was uses (as seen in Figure 3.1). Particles were generated using a TSI atomizer (Model 3076, Shoreview, MN) with an ~1% (vol.) solution of bis(2-ethylhexyl) sebacate (DOS) in ethanol. The aerosol was then diluted by a factor of approximately 64 using two ejector diluters (DI-1000, Dekati Ltd, Kangasala, Finland), in series to evaporate the ethanol. This solution was selected as it generates spherical particles with a known density (910 kg/m^3). The width of the CPMA transfer function

is dependent on both of these properties (i.e. the transfer function is a function of the particle mobility), thus using this particle source allowed for the ideal transfer function to be calculated.

A potentially complicating factor in a tandem CPMA experiment is that uncharged particles may pass through the classifier when the rotational speed of the CPMA is low and the centrifugal force on small particles is very low. To prevent these particles from entering the CPMA, a DMA (TSI, Model 3080, Shoreview, MN) was used upstream of the tandem CPMAs to both charge particles (with the DMA's Kr-85 neutralizer) and eliminate any uncharged particles. As discussed in Section 3, the particle size distribution entering CPMA 1 should be broad, thus the resolution of the DMA was set to allow a broad range of particles through. The aerosol flow rate through the DMA and tandem CPMA system was 0.3 LPM, 1.5 LPM or 4 LPM. The DMA sheath flow was set to 1 LPM, 2 LPM and 5 LPM respectively for the previously stated aerosol flows resulting in a broad distribution entering CPMA 1. For measurements taken at 0.3 LPM and 1.5 LPM the aerosol flow rate was regulated using the internal flow control of the CPC (TSI, Model 3776, Shoreview, MN). For measurements at 4 LPM the CPC was set to a flow rate of 1.5 LPM and a vacuum pump with a critical orifice were used to regulate a makeup flow of 2.5 LPM, thus generating a net flow of 4 LPM through the tandem CPMAs.

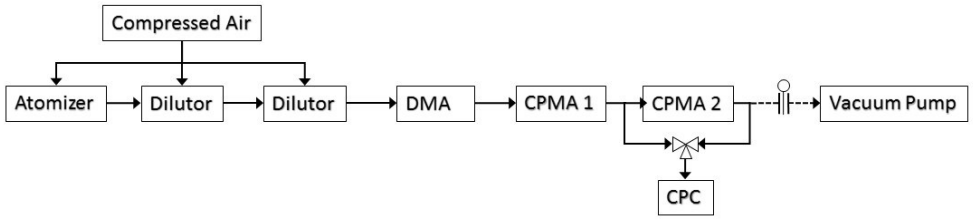

Figure 3.1: Schematic of tandem CPMA experiment.

Once the particles were classified by the DMA, the aerosol enters CPMA 1 which was set at a constant mass set point of 0.01 fg, 0.1 fg, 1 fg, 10 fg or 100 fg (assuming the particles are

singly-charged). The DMA set point was chosen to select the equivalent diameter for each mass set point (27 nm, 60 nm, 128 nm, 275 nm, 593 nm) to maximize the number of particles entering CPMA 2. CPC measurements were then taken downstream of CPMA 1 to determine the steady state particle concentration leaving CPMA 1. The CPC was then connected downstream of CPMA 2, and CPMA 2 was stepped through a range of mass set points and the CPC measured the particle concentration exiting CPMA 2 (*i.e.* CPMA 2 was set to a mass set point for several seconds to record the particle concentration then it was set to a new set point.)

The CPMAs (Cambustion Ltd., Cambridge, UK) were tested at each particle mass (0.01 – 100 fg) and each flowrate (0.3 – 4 LPM), at a resolution of 3, 5 or 10 if the operating condition was within the operating window of the CPMA (i.e. some operating conditions could not be tested because they would exceed the maximum or minimum voltage or rotational speed of the CPMA). The resolution is defined as the inverse of the full-width half-maximum of an ideal triangular transfer function (Flagan 2011). Some set points at high rotational speeds (*e.g.* 0.01 fg) were left out even though they were within the operating window of the CPMA as the temperature of the CPMA would rise (> 60 ^{o}C), potentially causing some evaporation of the DOS particles. In some experiments at 0.01 fg the mass measured by CPMA 2 was substantially lower than the mass set point of CPMA 1, indicating that particle evaporation was occurring. Thus, limiting the temperature of the CPMA (by starting the test when the CPMA was cool) prevented the aerosol from partially evaporating and changing mass.

Two separate CPMA's were used which are designated as "CPMA A" (serial number C220) and "CPMA B" (serial number C313). Each experiment was repeated with each CPMA in the CPMA 1 and CPMA 2 positions.

3.3 Theory

The CPMA transfer function can be either trapezoidal or triangular in shape. The shape of this transfer function is determined by the speed ratio and radii ratio of the two cylinders in the device. Any imperfection within the cylinders of the CPMA, the effects of diffusion, and a difference in rotational speed of the inner and outer cylinders of the CPMA from the expected values, may cause deviations from the expected transfer function. There are two scenarios that produce "stable" transfer functions within the CPMA. They are dependant on the following:

$$\omega_{\text{inner}}\, r_{\text{inner}} \geq\ \omega_{\text{outer}}\, r_{\text{outer}} \qquad [6]$$

where ω_{inner} and ω_{outer} are the inner and outer cylinder rotational speeds, and r_{inner} and r_{outer} are the inner and outer cylinder radii. When the two sides of equation 6 are equal the transfer function of the CPMA is neutrally stable (*i.e.* particles with a mass equal to the CPMA mass set point will have equal centrifugal and electrostatic forces acting on them regardless of radial position (Olfert and Collings 2005), which produces an approximately triangular transfer function). When the inequality of equation 6 is true, the transfer function becomes positively stable (*i.e.* particles with a mass equal to the CPMA mass set point will converge toward the middle of the gap between the cylinders), which produces a trapezoidal transfer function. (In the APM, the forces are always unstable, and particles diverge toward the cylinders walls, reducing the penetration efficiency of the classifier). The dimensions of the commercial CPMA are an outer radius of 61mm, an inner radius of 60 mm and a speed ratio ($\omega_{\text{outer}}/\omega_{\text{inner}}$) of 0.9696. This produces a slightly positively stable scenario and thus the CPMA produces a slightly

trapezoidal transfer function, as shown in Figure 3.2, calculated using the non-diffusion model of (Olfert and Collings 2005).

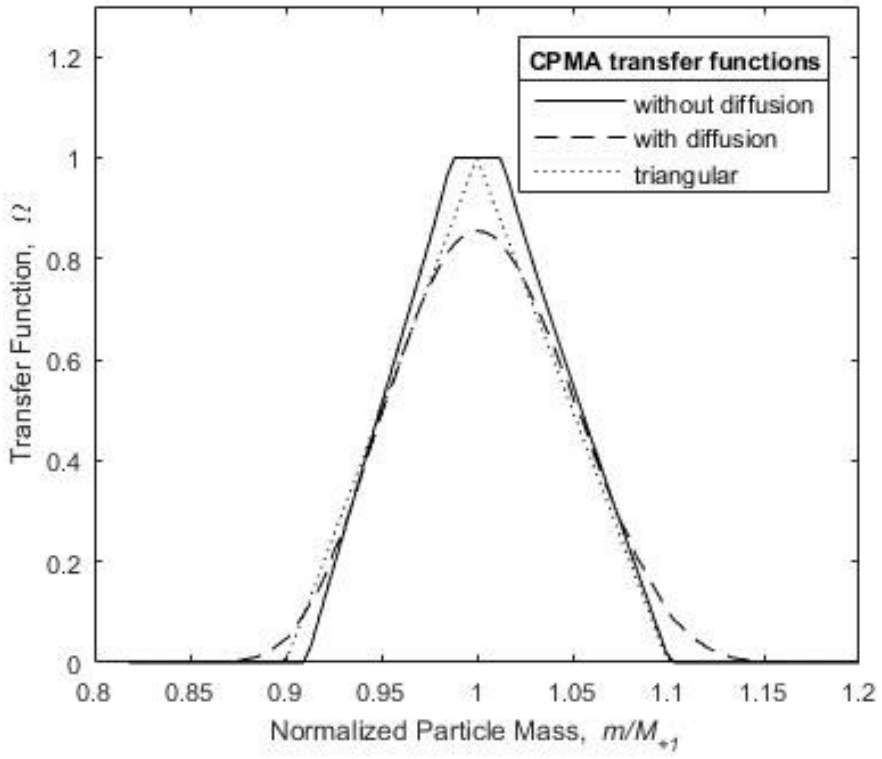

Figure 3.2: Normalized transfer function of the CPMA with and without diffusion for a setpoint of 0.01 fg (27 nm), and a triangular transfer function.

Figure 3.2also shows the theoretical transfer function including the effects of particle diffusion (for a particle size of 27 nm using the model of Olfert and Collings (2005) and an ideal triangular transfer function with the same resolution as the trapezoidal transfer function. Even though the CPMA produces a trapezoidal transfer function, it is typically assumed to be triangular in shape. Assuming the triangular transfer function simplifies data analysis greatly in many applications (including data inversion to reconstruct aerosol distributions) and when evaluating the convolution of two transfer functions, as is necessary for the analysis of the CPMA in this experiment. Thus, in this study we will experimentally investigate how the

experimental transfer function differs from the triangular transfer function, which we will call the 'ideal' transfer function.

Martinsson et al. (2001) have characterized the ideal transfer function with three parameters, the height at the instrument set point (h), the full width half maximum ($FWHM$), and the area of the transfer function (A). For the ideal transfer function these can be defined as follows:

$$h = 1$$

$$FWHM = \frac{M_{+1}}{R_m} \quad [7]$$

$$A = h \cdot FWHM$$

where R_m is the resolution of the CPMA and M_{+1} is the mass set point of the CPMA.

As previously stated, there are a number of items that affect the shape of the transfer function. As such, parameters can be introduced that can properly represent some of these non-ideal scenarios. These parameters provide a method to determine the level of non-ideal behavior of the CPMA; the further the values are from one, the more non-ideal the transfer function. However, for the purposes of the CPMA-electrometer system the item of concern is the mass setpoint. As such, the variables that will be introduced will be used to determine the variation in this value.

The set point of the CPMA is based on two forces, the centrifugal force and the electric force. Balancing these two forces, the mass (m) to charge (n_q) ratio, or the mass setpoint (M_{+1}), is (Olfert et al. 2006),

$$\frac{M_{+1}}{n_q} = \frac{eV}{r_c^2 \omega_c^2 \ln\left(\frac{r_{outer}}{r_{inner}}\right)} \quad [8]$$

where e is the charge of an electron (1.6 x 10^{-19} C), V is the voltage difference between the cylinders, r_c is the center radius between the two cylinders, and ω_c is the rotational speed at radius r_c . In equation 8, there are only two parameters that are user-controlled, the rotational speed ω_c, and the voltage V. As such, the user can vary these two items to select for the required mass, where different combinations of these parameters will change the resolution of the CPMA.

The resolution of the CPMA is defined as the inverse of the normalized full-width half maximum of the transfer function (a similar definition is often used with DMA transfer functions; Flagan 2011). For a triangular transfer function the resolution is,

$$\frac{1}{R_m} = \frac{m_{max}}{M_{+1}} - 1 \quad [9]$$

where m_{max} is the maximum mass that passes though the CPMA and is,

$$m_{max} = \frac{1}{\omega_c^2 r_c}\left[\frac{Q}{2\pi B_{max} L r_c} + qE\right] \quad [10]$$

where Q is the flow rate through the CPMA, L is the length of the cylinders, E is the electric field and B_{max} is the mobility of a particle of mass m_{max}. As such, this is a recursive function as B_{max} is a function of m_{max} (Cambustion 2015). Using equation 9 and equation 10 the

resolution of the device can be found. These relations assume the channel is narrow enough such that the forces do not vary across the gap. In addition to this, it is also assumed the charge on all particles is equal and the velocity profile is uniform across the channel. The resolution of the commercial CPMA is calculated using these assumptions and calculations.

Knowing both the set point, and resolution of the CPMA allows for the ideal transfer function of the CPMA to be non-dimensionalized following (Stolzenburg and McMurry 2008) for the general equation for a triangular transfer function.

$$\Omega = \frac{R_m}{2}\left[\left|\frac{m}{M_{+1}} - \left(1 + \frac{1}{R_m}\right)\right| + \left|\frac{m}{M_{+1}} - \left(1 - \frac{1}{R_m}\right)\right| - 2\left|\frac{m}{M_{+1}} - 1\right|\right] \quad [11]$$

where m is an arbitrary particle mass that ranges from 0 to any positive value. This equation governs the ideal transfer function of the CPMA based on the user controlled inputs (R_m and m_0).

The mass setpoint of the CPMA is determined using the tandem CPMA experiments described in Section 4.2. In these experiments CPMA 1 is held at a constant set point and CPMA 2 is stepped while the concentration exiting CPMA 1 (N_1) and CPMA 2 (N_2) is recorded. An example set of experimental data is shown in Figure 4. The resulting concentration ratio (N_2/ N_1) is the result of the convolution of the two CPMA transfer functions assuming that the distribution of particles entering CPMA 1 is uniform. The figure shows the convolution of two ideal triangular transfer functions (solid line) and the experimental data. Note that the experimental data has a lower amplitude, a slightly narrower width, and a slight offset relative to the ideal case caused by non-idealities of the transfer functions as well as differences in the mass set points between the two CPMAs (potentially due to differences in voltage and rotational speed

calibrations, etc.). The offset between the two CPMA set points can be quantified by the parameter ψ where $\psi = M_{+1,2}/M_{+1,1}$, and $M_{+1,1}$and $M_{+1,2}$ are the mass set points of CPMA 1 and CPMA 2 respectively. In addition to this, two other parameters can be defined to represent the decrease in amplitude (λ) or variation in width (μ) of the transfer function. These have been defined in such a way that equation 11 can be re written as:

$$\Omega = \frac{\lambda\mu^2 R_m}{2}\left[\left|\frac{m}{M_{+1}} - \left(1 + \frac{1}{R_m\,\mu}\right)\right| + \left|\frac{m}{M_{+1}} - \left(1 - \frac{1}{R_m\,\mu}\right)\right| - 2\left|\frac{m}{M_{+1}} - 1\right|\right] \qquad [12]$$

The mass parameters (ψ) was found by convolving the non-ideal transfer functions (Eq 12) and adjusting the three parameters (ψ, μ, λ) using χ^2 minimization to fit the experimental data. The minimization routine was program in Matlab using the fminsearch function. The figure shows that the non-ideal convolution (dashed line) fits the data well suggesting that the triangular transfer function (adjusted by the three parameters) is a reasonable approximation of the actual CPMA transfer function. In the analysis it is assumed that all particles are singly charged. If multiple charges are present, the mobility of these particles is higher than the singly-charged particles; as such, the convolution of the two CPMA transfer functions with multiple charges has a broader distribution near the base. Analysis was conducted to determine the likelihood of multiple charges to be present and can be found in Appendix A. From the analysis

it is shown that the likelihood of multiple charges affecting the fit is negligible.

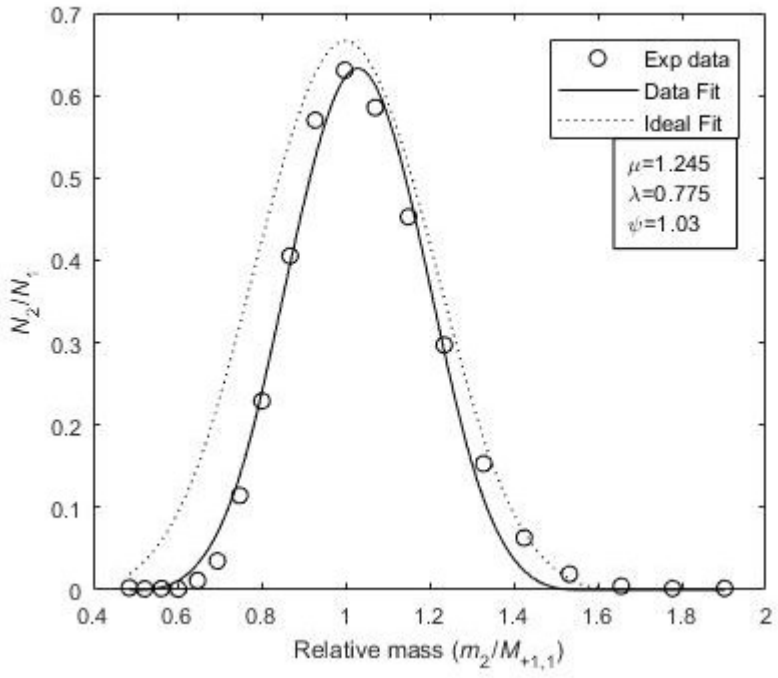

Figure 3.3: Sample data set and output. Set point of 10 fg and a resolution of 3 was used at 1.5 LPM.

3.4 Results and Discussion

Figure 3.4 displays the results for the offset parameter for the two devices. The error bars on the plots represents the uncertainty in the mean of the measurements with 95% confidence. Each data point for a device is calculated when the respective CPMA was in position 2 as identified in Figure 3.1. The figure shows the mass offset based on mass set point and device even though the effects of flow rate and resolution were also examined. It was found that there was little systematic difference when varying the flow rate and resolution, the level of variation appeared to be caused by the random nature of the measurements. For small particles it is much more likely to have variation in the measurements with regards to the parameters examined. In particular, diffusional losses of small particles should increase for low flow rates in the classifier. However, due to the limits of operational window of the CPMA, with a mass set point of 0.01 fg

(particle diameter, *d*, of 27 nm), only one set of conditions was tested (0.01 fg, at 0.3 LPM and a resolution of 3). As such, no variation between set points (with regards to resolution or flow rate) could be detected.

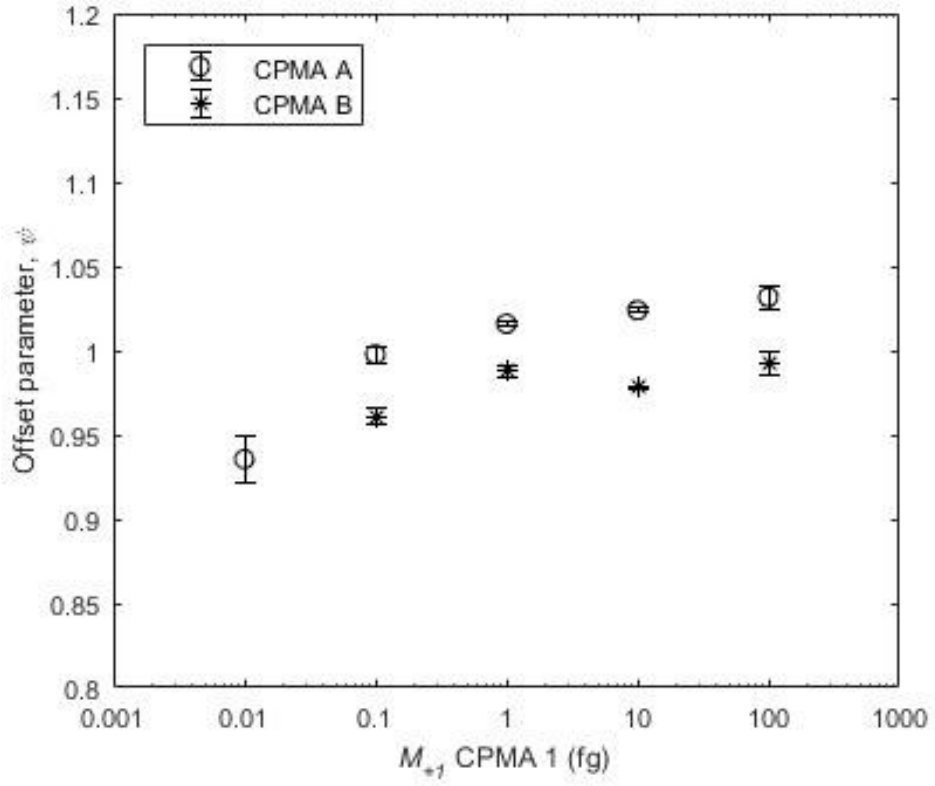

Figure 3.4: Mass offset measurement for the transfer function of the two CPMA's. Measurements were made with each respective CPMA in position 2 as identified by Figure 3.1.

Figure 3.4 displays the offset parameter for the two CPMA's. The figure displays the ratio between the set point of the CPMA in position 1 and the apparent set point of the CPMA in position 2 as found by the convolution of the transfer functions. As such, this displays the relative offset between the two devices. The ideal case occurs when a value of 1 is found. It is important to note that the difference between the two devices in one test is not the difference

between two points shown in the figure. For example, for the set point of 1 fg, CPMA A had an offset parameter of 1.016 while CPMA B had an offset parameter of 0.988. This means that for a set point of 1 fg, the expected deviation between the CPMA's is less than 2%. Due to the nature of the experiment it is expected the data should be symmetric around a value of 1 (i.e. when the CPMA positions are switched it is expected that the magnitude of the offset to be the same but in the opposite direction). For particle masses greater than or equal to 1 fg, CPMA A has mass offset that is slightly larger than one while CPMA B gives an offset that is slightly less than one, and they are approximately symmetric about one, as expected.

For the set points of 0.1 fg and 0.01 fg the mass offset of CPMA A is below one. This is likely caused by particle evaporation occurring within the second CPMA as the particle mass will decrease as it travels though CPMA 1 and CPMA 2. A decreasing mass through the system is represented by a decrease in the offset parameter. This might be expected as the smaller mass set points have higher rotational speeds and thus the devices operate at higher temperatures making it possible that for the lower set points the DOS may have begun to evaporate and thus reduce the mass of the particles.

A summary of the data with regards to all set points for CPMA A and CPMA B can be found in Appendix B (this data represents the repeatability of the CPMA). Figure 3.5 displays this data with relation to each set point. From this figure it can be found that all of the data except for 3 points fall below 0.02 (with the majority of the high points near 0.02 being found at 100 fg set point). Overall, the average of these repeatability's is 0.8%.

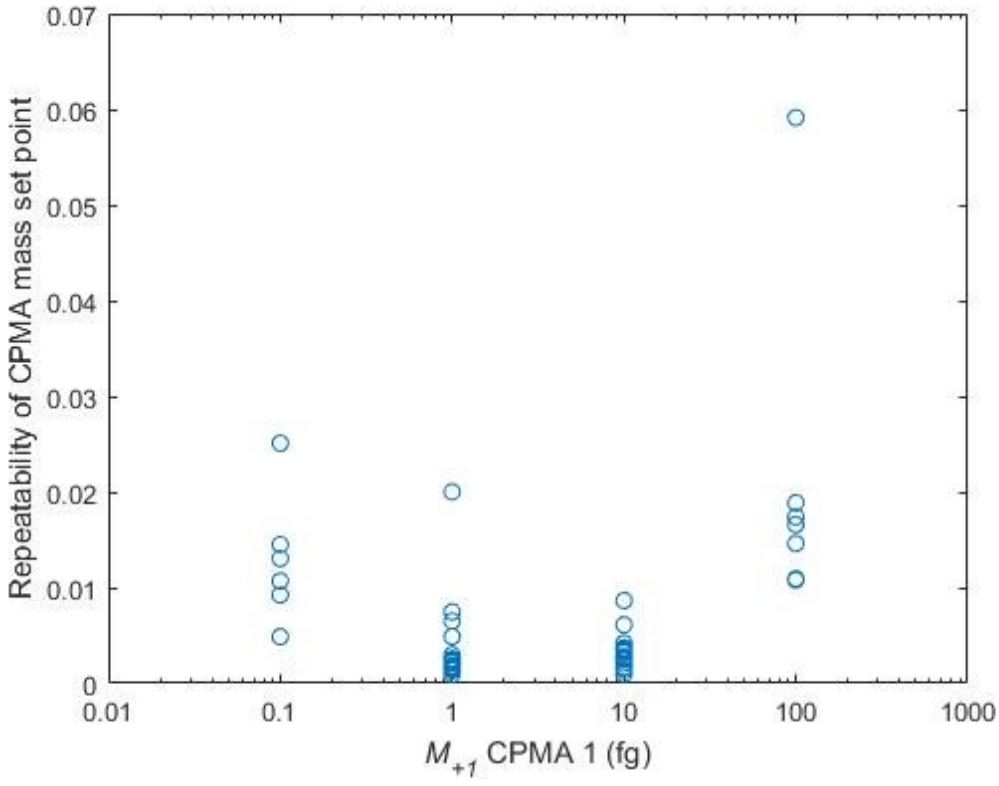

Figure 3.5: Repeatability of CPMA in tandem CPMA-CPMA experiment. Repeatability was calculated when devices were in position 2 of Figure 1

The intermediate precision taking into account all data points collected can be calculated as 0.013 or 1.3%. The intermediate precision of the above testing procedure is M=2, as testing took place with two devices, on various days. The following chapter will examine the other components of the CPMA-electrometer setup and the overall CPMA-electrometer setup in terms of reproducibility and intermediate precision.

Chapter 4 Testing Procedures

To determine the repeatability and intermediate precision of the CPMA-Electrometer system a number of tests were conducted. Each test examined one or more components of the overall set up other than the CPMA as that was previously studied in chapter 3; by determining the variability of each of the individual components, a prediction can be made as to the variability of the overall setup. As was previously stated, the major components that were tested are as follows: flow controllers, electrometers, Faraday cups and CPMAs. Each of these components were tested using a different experimental set up, which will each be described in the following sections. All of the devices were tested using the previously defined criteria for repeatability and intermediate precision.

4.1Flow Controller Repeatability and Intermediate Precision

The flow controllers are required to maintain a steady flow of air though the Faraday cup. Deviations from the expected value will alter the current readout of the electrometer and thus the mass concentration.

4.1.1 Setup

The flow controllers were tested by measuring the controlled flow, daily, though the device. This was accomplished using a Gilibrator bubble flowmeter (serial 0209522-5) to calibrate each of the two flow controllers. Each device was calibrated with a set point of 4.0 SLPM at 0˚C and 1 atm on the first day of testing. The actual flow rate through the flow controllers was then measured on each day of testing. Figure 4.1 displays the schematic what was used to calibrate the flow controllers. Both flow controller 1 and flow controller 2 (both of

the flow controllers downstream of the Faraday cups from each of the two systems tested) were tested using this method.

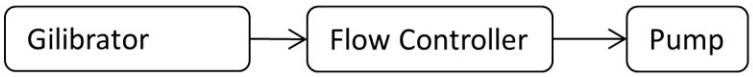

Figure 4.1: Test schematic for flow controller repeatability and intermediate precision measurements.

4.1.2 Results

The results for each of the two flow controllers tested can be seen in Figure 4.2. The set point for each device was initially 4.0 SLPM (4000 cm^3/min). The largest repeatability for system 1 occurred on February 2nd and had a value of 10 cm^3/min (0.25%). The largest bias for system 1 occurred on February 1st and had a value of 32 cm^3/min (0.8%). For system 2, the largest repeatability occurred on February 1st with a value of 8 cm^3/min (0.19%). For system 2, the largest bias occurred on February 4th with a value of 9 cm^3/min (0.23%). In addition, the time-different intermediate precision for each system was calculated. System 2 had a found value of 7 cm^3/min (0.17%), while system 1 had a time-different intermediate precision of 16 cm^3/min (0.39%). Overall, the time-and-equipment-different intermediate precision for the two flow controllers was 12 cm^3/min (0.311%). These are all relatively small values, making the flow controller an unlikely source of error. However, it can be expected that the accuracy of the flow controllers will have an error of less than 1%.

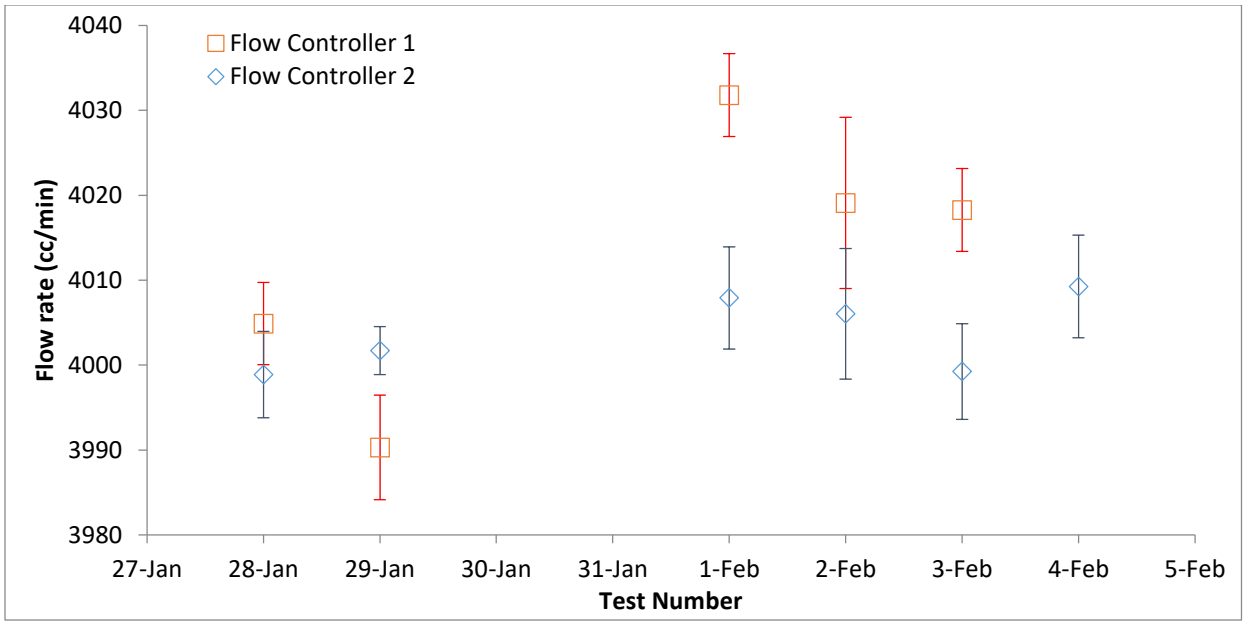

Figure 4.2: Repeatability and intermediate precision measurements for the two flow controllers, each from a separate CPMA-electrometer setup. Error bars represent the standard deviation for each data point. Each daily average consists of 10 individual measurements. All testing dates were in 2016.

4.2 Electrometer Repeatability and Intermediate Precision

The electrometer is required to measure the generated current between the two cups of the Faraday Cup. As such, any deviation from the true value will directly affect the measured mass concentration. Accurate measurements are necessary from this device to ensure measurements can be trusted.

4.2.1 Setup

The bias in the two electrometers was found by calibrating each of the two devices with a reference standard. This was achieved by applying a known voltage, from a high accuracy voltage source, across a known resistor, and measuring the current that is produced. For the test, the voltage was varied from -0.20 V to 0.20 V (accuracy less than 0.01%); the resistor used was a 10 GΩ resistor (accuracy less than 0.01%). As such, the expected current range was from -20 to 20 pA.

4.1.2 Results

The data that was collected from each of the electrometers is displayed in Figure 4.3. It is expected that the slope of the line of best fit will be 1. Any deviation from this slope is related to the measurement error of the device. From Figure 4.3 it can be seen the electrometer 1 had a bias error of 1.9% while electrometer 2 displays a bias of 1.2%.

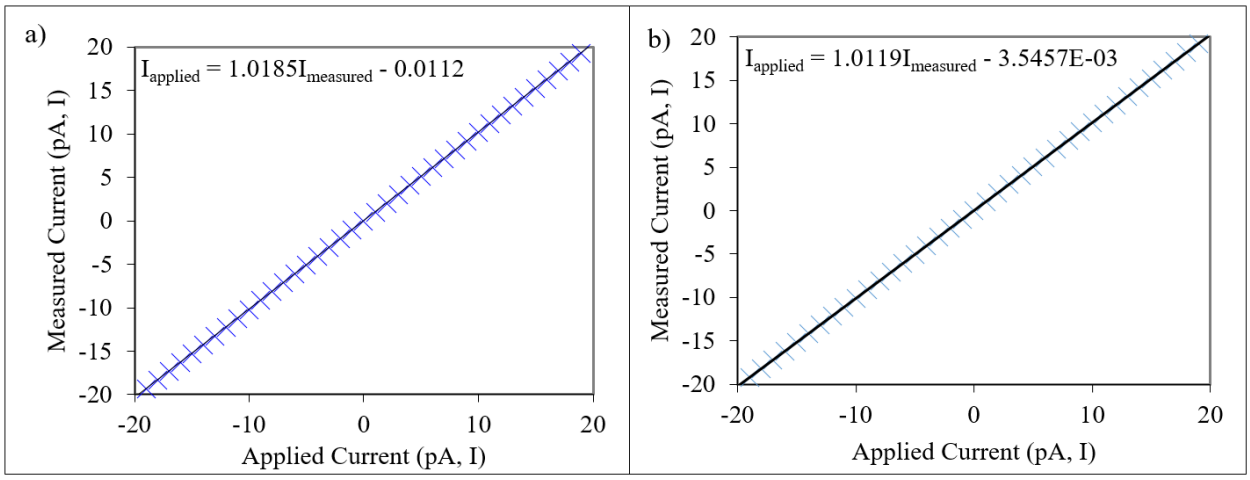

Figure 4.3: Electrometer calibration results for a) electrometer 1, and b) electrometer 2.

The residuals of the two plots above were also found and can be seen in Figure 4.4. The residuals for electrometer 2 resemble what is expected. The residuals are randomly scattered and are of a low magnitude. Electrometer 1 however displays a trend that is lowest for a current of ±10pA and gets larger the further away the current is from this value. Taking these values as a percentage, it can be found that as long as the current reading is greater than 1 pA, the bias is less than 0.3%.

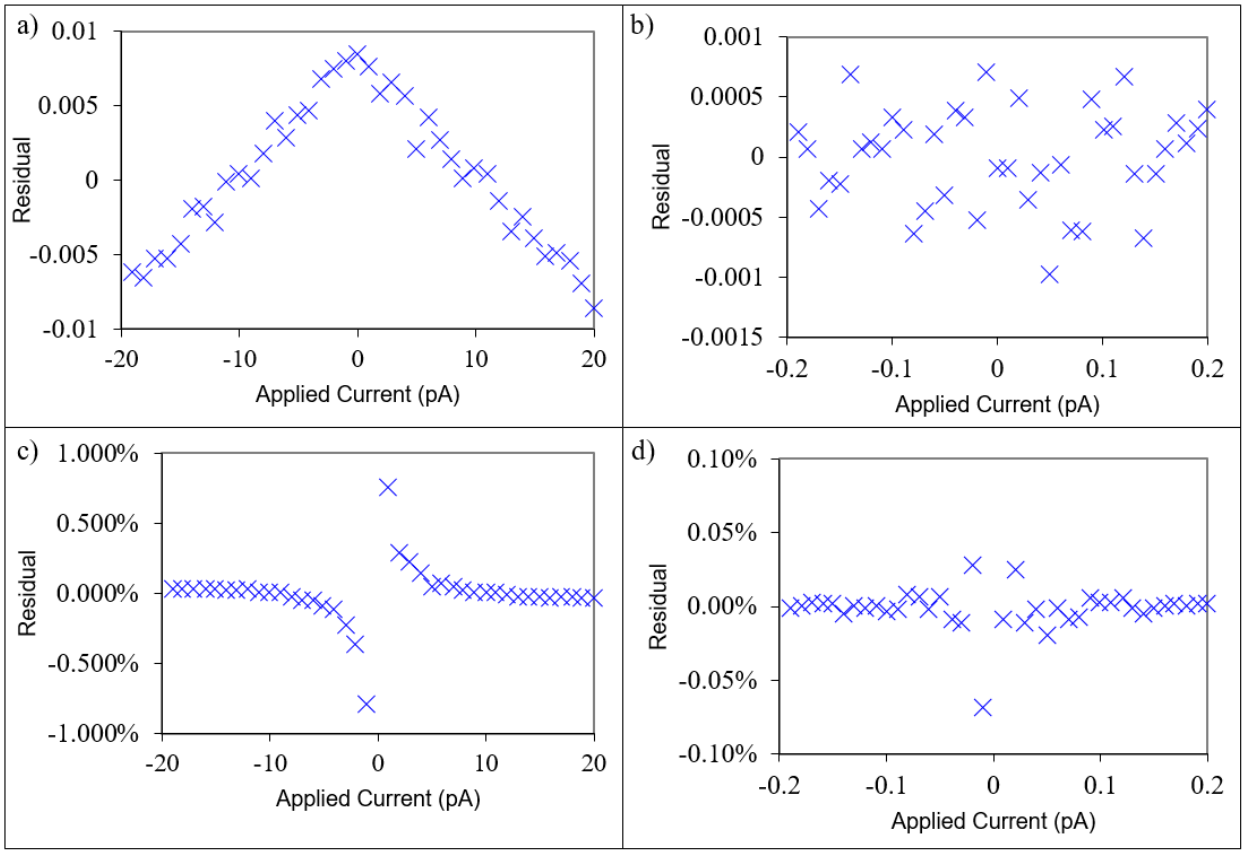

Figure 4.4: Residual plots for electrometer tests. a) and b) display the residuals as a current offset for electrometer 1 and 2 respectively. c) and d) display the same plots but as a percentage of the applied current.

4.3 Faraday Cup Repeatability and Intermediate Precision

While the Faraday cup captures the charge on the aerosol, it does not directly measure the current. As such, the Faraday cup repeatability and intermediate precision are affected by any uncertainty present in the electrometer as well. These measurements were collected and determined the overall repeatability and intermediate precision of the Faraday cup-electrometer system as a whole.

4.3.1 Setup

A method to individually test the Faraday cup by measuring an accepted standard is not known. Therefore, to determine the response of the Faraday Cup, a test was conducted to compare between the two Faraday cups.

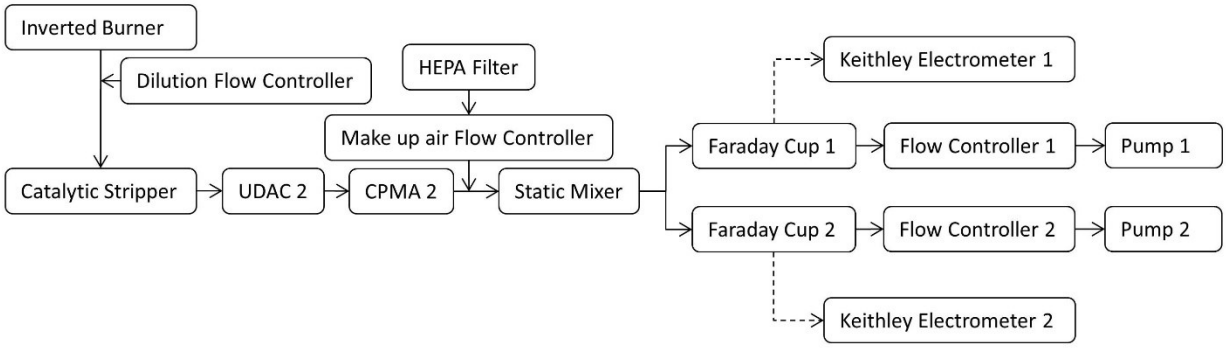

Figure 4.5: Schematic for Faraday Cup testing.

Figure 4.5 displays the testing schematic that was used for the Faraday cup comparison. For each test, components from either system 1 or system 2 were used when there was a choice. All other equipment was system 2's equipment. Testing was repeated for both Faraday cup's, each day, for a total of 4 days. The inverted burner had a fuel flow rate of 1.4 liters per minute, combustion air at 16.6 liters per minute, and dilution air at a flow rate of 200 liters per minute. The burner was provided ample time (>1 hour) to warm up and provide a stable particle distribution.

The soot was then passed through a Cambustion Unipolar Diffusion Aerosol Charger (UDAC). Upon charging, the flow traveled through a Cambustion Centrifugal Particle Mass Analyzer (CPMA). The CPMA was used to classify the particle distribution for all particles with a mass to charge ratio of 0.25 fg/charge and a resolution of 5.0. 0.25 fg/charge was selected as this was to the left of the peak of the particle distribution for the inverted burner used. This provides a large mass concentration for a single set point while limiting the number of uncharged particles. These particles then traveled through the Faraday cup where the charges were transferred to the Faraday cup, and the induced current measured by the Keithley Electrometer.

4.3.2 Results

Figure 4.6 displays the data collected over the four days of testing. The slopes all closely resemble the data indicated by the large R^2 values. If the data is all displayed on the same plot, the average trend line can be found. This is displayed in Figure 4.7. All of the data falls on a straight line, as can again be seen by the slope of 1.0468 (pA/pA) and an R^2 value of 0.9995. Table 4.1 displays a summary of the slopes for each line of best fit, as well as the % difference each slope is from the average slope of 1.0468.

For this experiment the time and instrument different intermediate precision can be found similarly to the analysis that was conducted in chapter 3. On each day of testing a line of best fit was found and a slope generated. As such, an expected value for system 1 can be obtained by taking systems 2 found value at the same point and using it in the equation of best fit. The repeatability was found by taking the standard deviation of normalized measurements for one device on one day. The repeatability for each test can be found in Table 4.1. The majority of testing had a repeatability of less than 0.008 (0.5%) however, testing that occurred on January 21st had the largest repeatability for both systems of 0.010. A full break down of the values used to calculate the M=1 intermediate precision can be found in appendix C.

The M=2 intermediate precision was calculated in a similar manner, however, all of the collected data points were used for the single calculation. This method gives an M= 2 intermediate precision for the Faraday cup-electrometer system of 0.022 (2.2%). The overall slope was 1.0468. The offset from this of 0.0468 (from the expected value of 1) on average relates to a systematic offset between the two systems. Note that relative offset between flow meters is <1% and the relative offset between electrometers is <1% so there must be some systematic difference between the two cups.

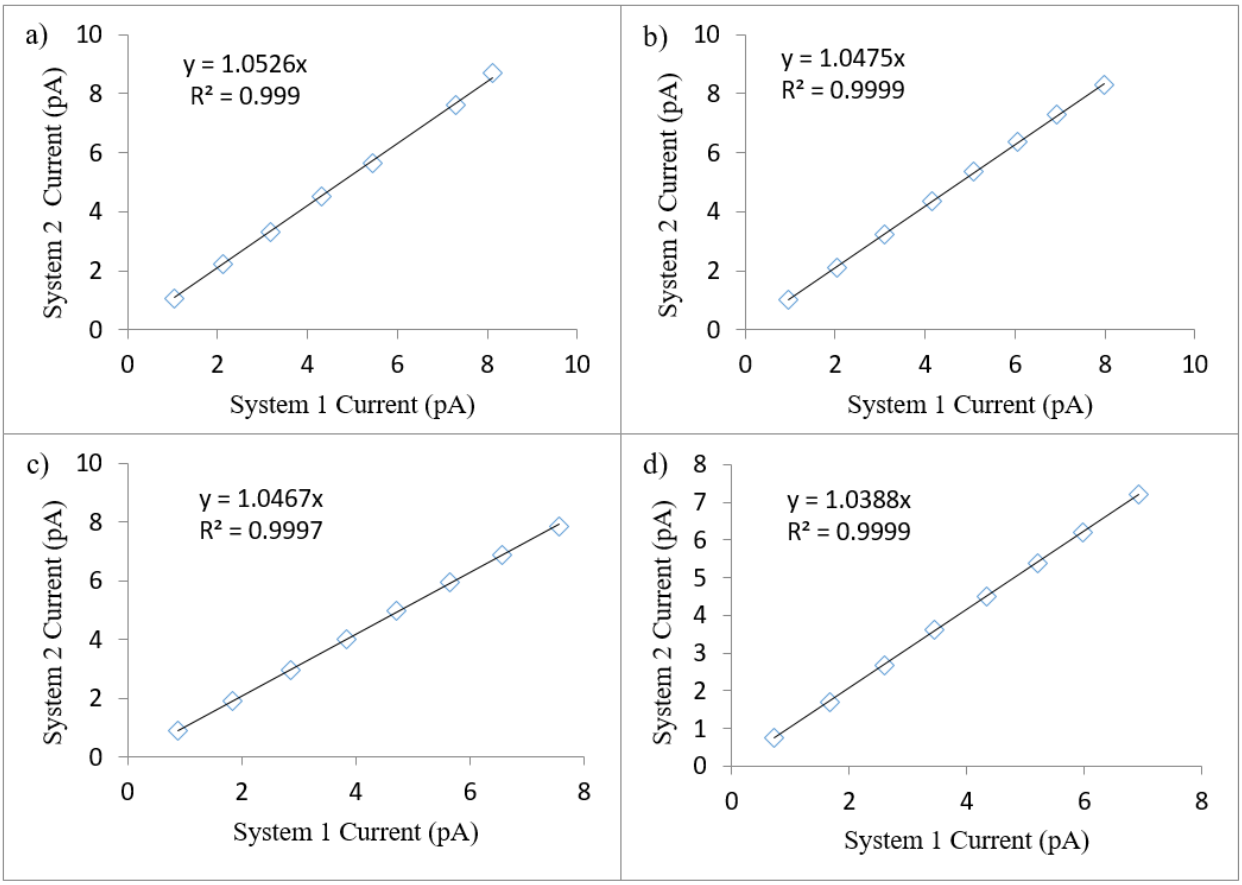

Figure 4.6: Faraday Cup test results from four days of testing a) displays the results measured on January 21st 2016. b) was from January 22nd 2016, c) was from January 25th 2016, and d) was from January 26th 2016. Each plot is comparing Faraday Cup 1 (on the x-axis to Faraday Cup 2 (on the y-axis).

Table 4.1: Summary of Slopes and repeatability for Faraday Cup testing.

Date	Slope	% Difference From Average	System 1 Repeatability (%)
Jan-21	1.0526	0.55%	0.010
Jan-22	1.0475	0.07%	0.007
Jan-25	1.0467	0.01%	0.008
Jan-26	1.0388	0.76%	0.006

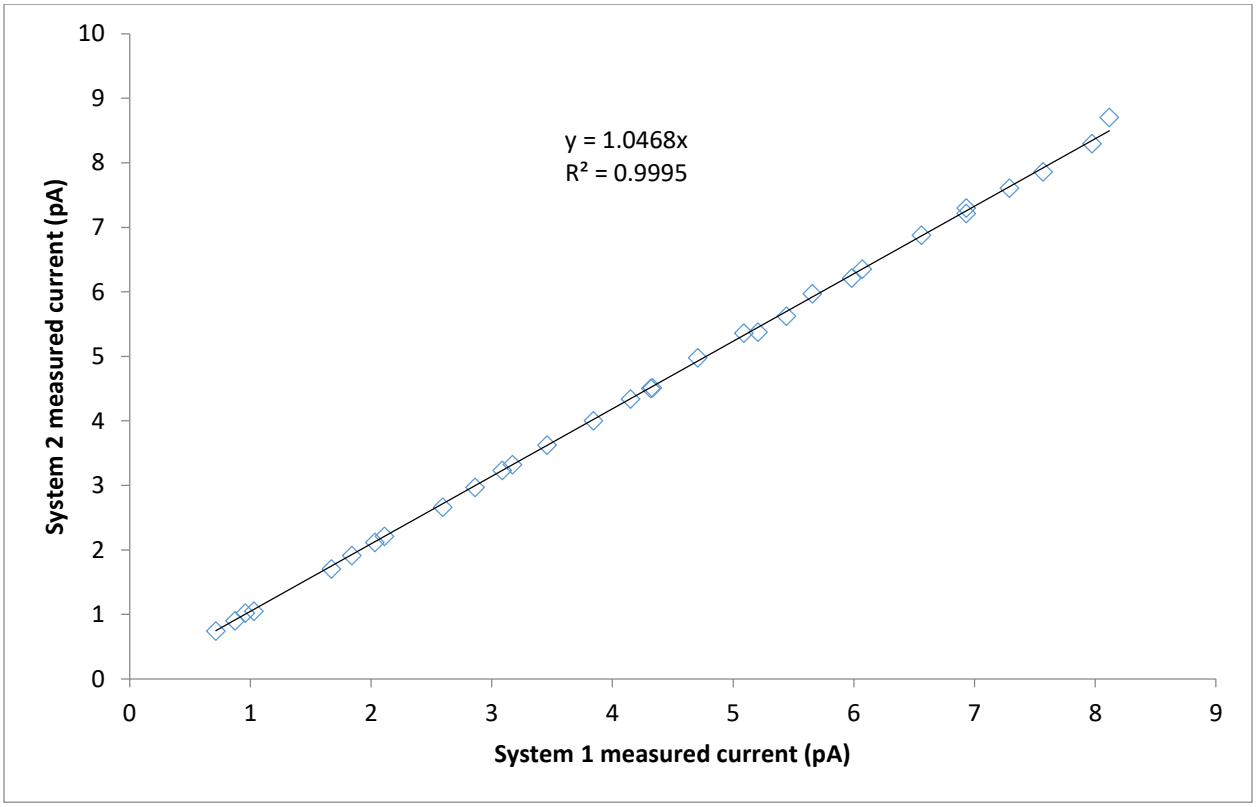

Figure 4.7: All data collected for Faraday Cup comparison experiments. The line of best fit presented is the line representing all data.

4.4 Intermediate precision and Repeatability of the combined CPMA-electrometer system

As was the intent of this project, the overall CPMA-electrometer was tested as one unit to determine the intermediate precision and repeatability. The testing of the individual components proved insight into any one component that may greatly affect the overall system such that

improvements can be made in the future to reduce the overall CPMA-electrometer systems repeatability and intermediate precision.

4.4.1 Setup

The testing to determine the intermediate precision and repeatability of a combined system of CPMA-electrometer and black carbon instrument using with either a Laser-Induced Incandescence instrument (LII) or a Cavity Attenuated Phase Shift Particulate Matter Single Scatter Albedo instrument (CAPS PMssa), as the challenge instrument. The testing schematic can be seen in Figure 4.8.

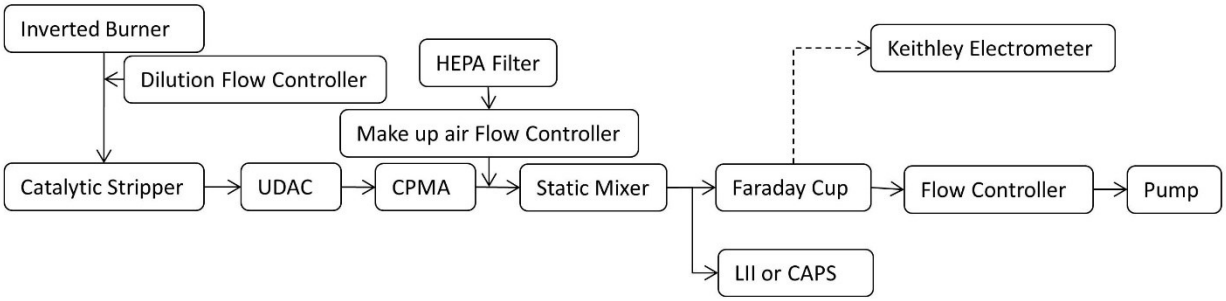

Figure 4.8: CPMA-electrometer intermediate precision and repeatability test schematic.

Testing was conducted over a period of multiple days, with multiple measurements being taken on each day. Tests were conducted by taking 8 (LII challenge instruments) or 9 (CAPS PMssa) different set points. Set points were achieved by adding extra dilution air to the sample line, after the Inverted Burner. This acted as a second stage of dilution and could be controlled during testing. This varied the concentration of the particles in the sampling line, thus the mass concentration was varied. Both the CPMA-electrometer system, and the challenge instrument saw the same changes in concentration. The values were then compared by plotting the CPMA-electrometer mass concentration against the challenge instruments mass concentration, and

determining the slope for the line of best fit. The slopes can then be compared to determine if the combined systems (both CPMA-electrometer and challenge instrument) are both repeatable and reproducible.

4.4.2 Results

Using the LII as the challenge instrument, two separate sets of data were collected. The first that will be examined is the one that looks at the repeatability of the combined CPMA-Electrometer/LII system. Figure 4.9 displays the repeatability measurements that were collected for CPMA-electrometer system 1 using the LII. For each individual day it can be seen that there is some slight variance (5%). The larger item of concern is the variation between days. This shifts from day to day, however, the largest change occurred between March 1st and March 2nd. The change in the slope between these two days was 0.09 (9%). This is a much larger variation than was previously seen with any one device that was previously tested. While this could mean that the CPMA-electrometer system is drifting, it is more likely that the LII measurements are drifting. This hypothesis can be supported by comparing the CPMA-Electrometer system to the CAPS PMssa.

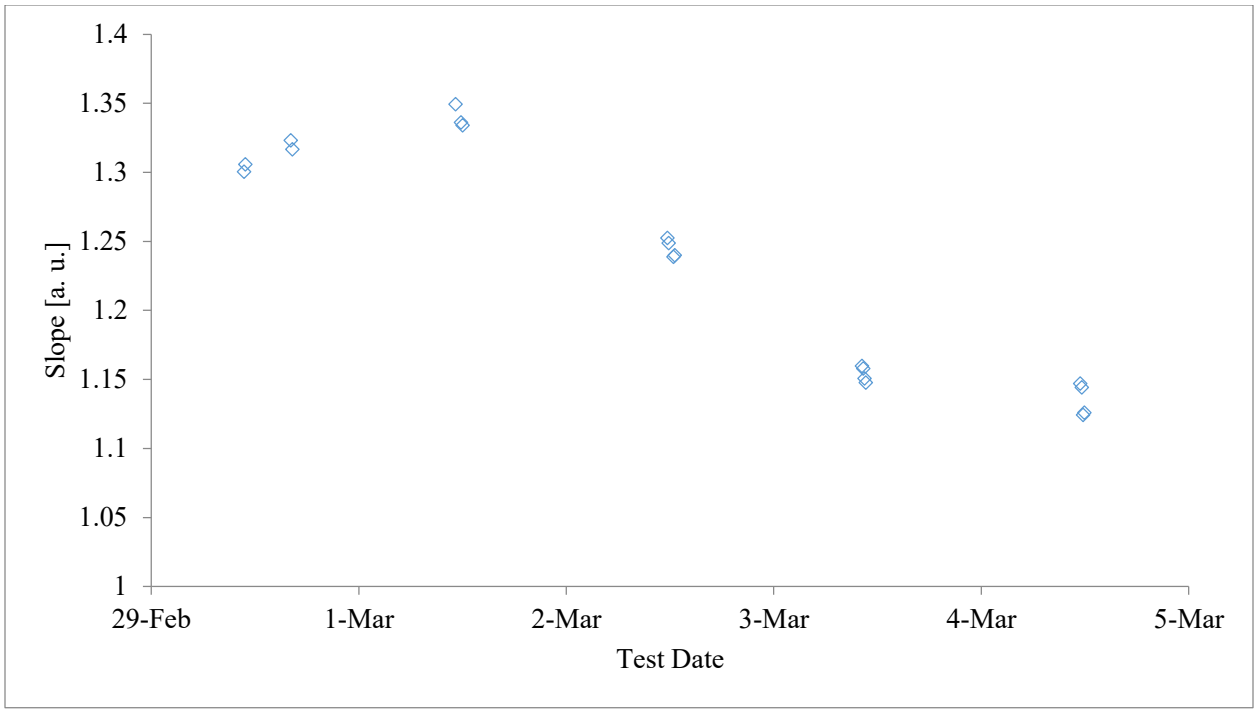

Figure 4.9: Repeatability data for CPMA-Electrometer system 1, with the LII as the challenge instrument.

Repeatability testing for system 1 was also conducted using a CAPS PMssa as the challenge instrument. The results from this test can be seen in Figure 4.10. This data set is much more stable than the comparison with the LII. On any one given day the slopes were all within 0.01 (1%) of the day's average. One item to note is that the data again from March 1st relatively higher. This spike however, only had an average difference of 0.05 (5%) between days. This could have been due to many factors including flame drift, or the CPMA-electrometer system had varied readings that day. Another item of note is the data displays a very small upwards drift for the average slopes on each day. This is the opposite direction of movement as compared to the LII slopes. As such, it is more likely that the LII was drifting rather than the CPMA-electrometer system in the tests shown in Figure 12.

The drifts measured in this system were much larger than any of the previously found bias or intermediate precision errors. It should be reiterated that the time-dependent

intermediate precision due to the flow meter was less than 0.5% and time-dependent intermediate precision of the Faraday cup was 0.5%. These items can only explain a portion of the larger error.

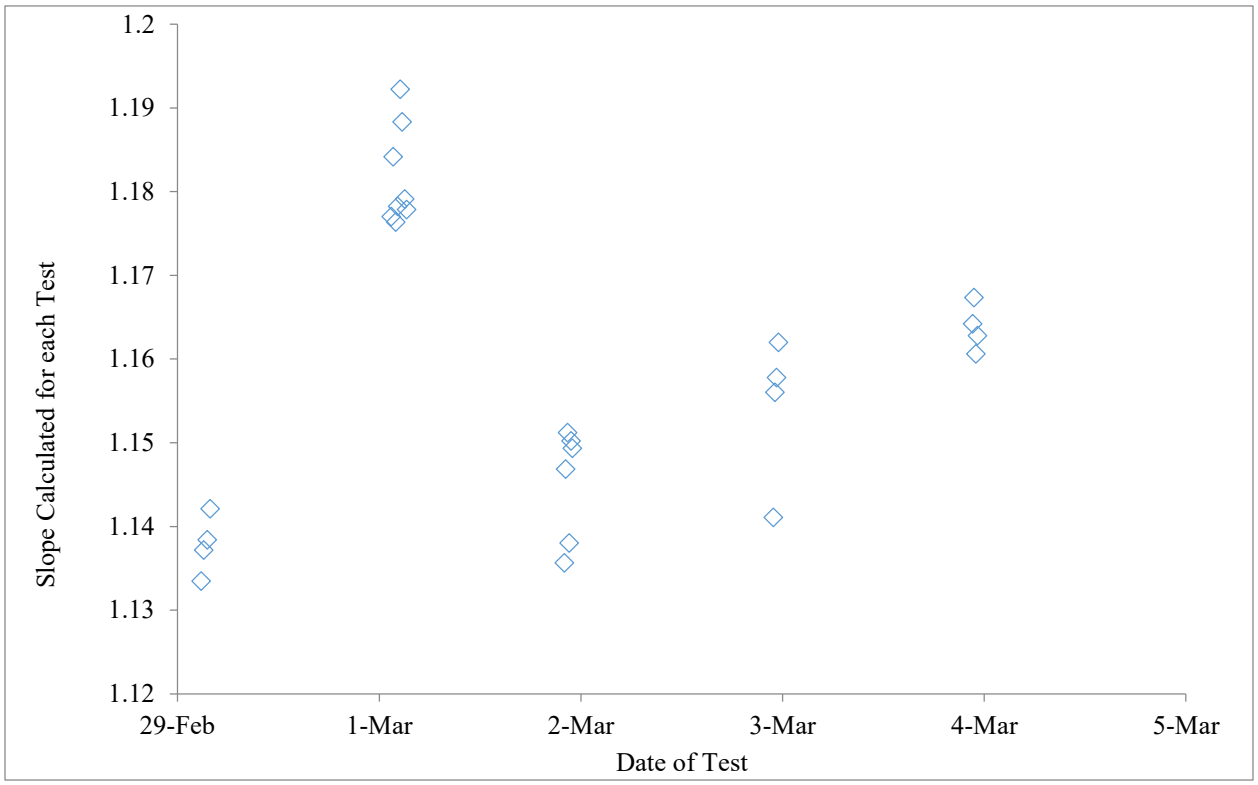

Figure 4.10: Repeatability measurements for CPMA-Electrometer 1, with CAPS PMssa as the challenge instrument.

Chapter 5 Conclusion

5.1 Summary

The testing that was conducted provides preliminary results that the CPMA-electrometer system is highly repeatable with limited sources of error. It was found that for the flow controllers, the accuracy of the devices has an error of less than 1%, while they were found to have a repeatability of less than 0.4% and an intermediate precision of *M*=2 of 0.3%. In addition, the bias error in the two electrometers was found to be less than 2% with a 1% difference between the two devices. Using these values, it was expected that the Faraday cup would likely have a bias between the two cups of less than 2%, due to the compounding bias of the flow controller and the electrometer. However, the time and device different intermediate precision for these two devices was slightly larger at only 2.2%. This increase in the intermediate precisions is likely caused by the offset between the two Faraday cups of 4.7%.

The tandem CPMA-CPMA test was conducted to determine the intermediate precision and repeatability of the CPMA itself. Testing was conducted by having one CPMA hold a mass/charge set point while the other scanned the expected range of particles. It was found that the repeatability of the CPMA was always less than 0.07, however, a good estimate for this value is less than 0.008 (0.8%) as this is the average repeatability. Overall, the *M*=2 intermediate precision of the CPMA was calculated as 0.013 (1.3%).

As was previously shown, the total mass concentration passing though the CPMA can be found as follows:

$$m_{\text{total}} = \frac{M_{+1} I}{Qe} \qquad [13]$$

Within this equation, a measure of the intermediate precision has been determined (assuming there is no uncertainty in the value of the elementary charge). The calculated values of the intermediate precision are related to the uncertainty of the device, as such, following error propagation an estimate of the intermediate precision of the overall system can be calculated. This procedure gives an estimate of the intermediate precision of 0.026 (2.6%); an improvement over NIOSH 5040. NIOSH (2003) states the NIOSH 5040 method has a i.e. repeatability of 8.5% at 23 $\mu g/m^3$ while Schauer et al. (2003) report a time, instrument, and laboratory-different intermediate precision between 6 and 21%.

The last tests conducted compared the whole CPMA-electrometer system to two separate challenge instruments. Only system 1 could be tested as CPMA 2 had a mechanical issue. When the challenge instrument was the LII, there was a large drift found which was likely due to the LII rather than the CPMA-electrometer system. The measured slope between the two devices was found to vary by up to 9%. As well, the variability within one day of measurements was up to 5%. With the CAPS PMssa as the challenge device the variation was much smaller. It was found that the day to day variation was only 5% and the within a test day that variation was 1%.

5.2 Future Work

There are a number of further tests which could be conducted in the future. The first item that requires action is the Faraday cup-electrometer testing could be repeated with a standard current flow such that the devices can be compared to a standard value, rather than be compared relative to each other.

There are a number of CPMA related tests that could be conducted. The tests that were run compared one CPMA to another, as such, the accuracy of the device could not be found. If both CPMA's that were tested have a bias towards a higher or lower value, the current tests

could not determine this. Using polystyrene latex spheres as the particle source of a known diameter (currently they are produced to a size of 20 nm) the mass set point of the CPMA could be accurately determined. By providing the CPMA with a flow of one particle size, the CPMA can then scan across the expected range of particles and the true difference in the set point of the CPMA can be determined.

Lastly, more testing could be done to determine the intermediate precision of the overall CPMA-electrometer system. This will provide critical information if the CPMA-electrometer system should be further investigated for sources of variability or if the challenge instrument should be inspected as a source of these variances. For the repeatability and intermediate precision, more data is required. The second CPMA had a mechanical failure and required repairs preventing this data from being collected. Once this is repaired data could be collected with CPMA-Electrometer system 2, which can then be used to collect more data and get a definitive answer about the intermediate precision of the CPMA-Electrometer system.

References

Bae, Min-Suk, James J. Schauer, Jeffrey T. DeMinter, Jay R. Turner, David Smith, and Robert A. Cary. 2004. "Validation of a Semi-Continuous Instrument for Elemental Carbon and Organic Carbon Using a Thermal-Optical Method." *Atmospheric Environment* 38 (18): 2885–2893.

Birmili, W., F. Stratmann, A. Wiedensohler, D. Covert, L. M. Russell, and O. Berg. 1997. "Determination of Differential Mobility Analyzer Transfer Functions Using Identical Instruments in Series." *Aerosol Science and Technology* 27 (2): 215–23. https://doi.org/10.1080/02786829708965468.

Biskos, G., K. Reavell, and N. Collings. 2005. "Unipolar Diffusion Charging of Aerosol Particles in the Transition Regime." *Journal of Aerosol Science* 36 (2): 247–65. https://doi.org/10.1016/j.jaerosci.2004.09.002.

Boucher, Olivier, David Randall, Paulo Artaxo, Christopher Bretherton, Graham Feingold, Piers Forster, V.-M. Kerminen, Yutaka Kondo, Hong Liao, and Ulrike Lohmann. 2013. "Clouds and Aerosols." In *Climate Change 2013: The Physical Science Basis. Contribution of Working Group I to the Fifth Assessment Report of the Intergovernmental Panel on Climate Change*, 571–657. Cambridge University Press.

Cambustion. 2011. "Centrifugal Particle Mass Analyser User Manual." Cambustion Limited.

Cambustion. 2012. "Unipolar Diffusion Aerosol Charger Manual 1.2." http://www.cambustion.com.

Cambustion. 2013. "Unipolar Diffusion Aerosol Charger Brochure." http://www.cambustion.com.

Cheng, Yung-Sung. 2011. "Condensation Particle Counters." Edited by Pramod Kulkarni, Paul A. Baron, and Klaus Willeke. *Aerosol Measurement: Principles, Techniques, and Applications* 381 (3rd Edition): 392.

Čokorilo, Olja. 2016. "Environmental Issues for Aircraft Operations at Airports." *Transportation Research Procedia* 14: 3713–20. https://doi.org/10.1016/j.trpro.2016.05.491.

Collins, D. R., D. R. Cocker, R. C. Flagan, and J. H. Seinfeld. 2004. “The Scanning DMA Transfer Function.” *Aerosol Science and Technology* 38 (8): 833–50. https://doi.org/10.1080/027868290503082.

Crutzen, Paul J. 2006. “Albedo Enhancement by Stratospheric Sulfur Injections: A Contribution to Resolve a Policy Dilemma?” *Climatic Change* 77 (3–4): 211–20. https://doi.org/10.1007/s10584-006-9101-y.

Dastanpour, R., S. N. Rogak, B. Graves, J. S. Olfert, M. L. Eggersdorfer, and A. M. Boies. 2016. “Improved Sizing of Soot Primary Particles Using Mass-Mobility Measurements.” *Aerosol Science and Technology* 50 (2): 101–9. https://doi.org/10.1080/02786826.2015.1130796.

DeCarlo, P. F., J. G. Slowik, D. R. Worsnop, P. Davidovits, and J. L. Jimenez. 2004. “Particle Morphology and Density Characterization by Combined Mobility and Aerodynamic Diameter Measurements. Part 1: Theory.” *Aerosol Science and Technology* 38 (12): 1185–1205. https://doi.org/10.1080/027868290903907.

Dhaniyala, Suresh, Martin Fierz, Jorma Keskinen, and Marko Marjamaki. 2011. “Instruments Based on Electrical Detection of Aerosols.” Edited by Pramod Kulkarni, Paul A. Baron, and Klaus Willeke. *Aerosol Measurement: Principles, Techniques, and Applications* 18 (3rd Edition): 393.

Dickau, M., T. J. Johnson, K. Thomson, G. Smallwood, and J. S. Olfert. 2015. “Demonstration of the CPMA-Electrometer System for Calibrating Black Carbon Particulate Mass Instruments.” *Aerosol Science and Technology* 49 (3): 152–58. https://doi.org/10.1080/02786826.2015.1010033.

Dickau, M., J. S. Olfert, M. E. J. Stettler, A. Boies, A. Momenimovahed, K. Thomson, G. Smallwood, and M. Johnson. 2016. “Methodology for Quantifying the Volatile Mixing State of an Aerosol.” *Aerosol Science and Technology* 50 (8): 759–72. https://doi.org/10.1080/02786826.2016.1185509.

Eggersdorfer, M.L., A.J. Gröhn, C.M. Sorensen, P.H. McMurry, and S.E. Pratsinis. 2012. “Mass-Mobility Characterization of Flame-Made ZrO2 Aerosols: Primary Particle Diameter and Extent of Aggregation.” *Journal of Colloid and Interface Science* 387 (1): 12–23. https://doi.org/10.1016/j.jcis.2012.07.078.

European Comission. 2011. “Commission Regulation (EU) No 852/2011.” *Official Journal of the European Union*.

Felber, Barbara, Antonio Valentin, Margherita Rosati, Cristina Bergamaschi, and George Pavlakis. 2014. “HIV DNA Vaccine: Stepwise Improvements Make a Difference.” *Vaccines* 2 (2): 354–79. https://doi.org/10.3390/vaccines2020354.

Flagan. 2011. “Chapter 15 in Kulkarni, P., Baron, P. A. and Willeke, K.” In *Aerosol Measurement: Principles, Techniques, and Applications*, 3rd ed. New Jersey: Wiley.

Högström, Richard, Paul Quincey, Dimitris Sarantaridis, Felix Lüönd, Andreas Nowak, Francesco Riccobono, Thomas Tuch, et al. 2014. “First Comprehensive Inter-Comparison of Aerosol Electrometers for Particle Sizes up to 200 Nm and Concentration Range 1000 Cm $^{-3}$ to 17 000 Cm $^{-3}$.” *Metrologia* 51 (3): 293–303. https://doi.org/10.1088/0026-1394/51/3/293.

Janssen, Nicole, and Weltgesundheitsorganisation, eds. 2012. *Health Effects of Black Carbon*. Copenhagen: World Health Organization, Regional Office for Europe.

Keith, David. 2013. *A Case for Climate Engineering*. 1st ed. MIT Press.

Landrigan, Philip J, Richard Fuller, Nereus J R Acosta, Olusoji Adeyi, Robert Arnold, Niladri (Nil) Basu, Abdoulaye Bibi Baldé, et al. 2017. “The Lancet Commission on Pollution and Health.” *The Lancet*, October. https://doi.org/10.1016/S0140-6736(17)32345-0.

Li, W., L. Li, and D. Chen. 2006. “Technical Note: A New Deconvolution Scheme for the Retrieval of True DMA Transfer Function from Tandem DMA Data.” *Aerosol Science and Technology* 40 (12): 1052–57. https://doi.org/10.1080/02786820600944331.

Magi, Brian I., Peter V. Hobbs, Thomas W. Kirchstetter, Tihomir Novakov, Dean A. Hegg, Song Gao, Jens Redemann, and Beat Schmid. 2005. “Aerosol Properties and Chemical Apportionment of Aerosol Optical Depth at Locations off the US East Coast in July and August 2001.” *Journal of the Atmospheric Sciences* 62 (4): 919–933.

Martinsson, B. G., M. N. A. Karlsson, and G. Frank. 2001. “Methodology to Estimate the Transfer Function of Individual Differential Mobility Analyzers.” *Aerosol Science and Technology* 35 (4): 815–23. https://doi.org/10.1080/027868201753227361.

McMurry, P. H., X. Wang, K. Park, and K. Ehara. 2002. “The Relationship between Mass and Mobility for Atmospheric Particles: A New Technique for Measuring Particle Density.”

Aerosol Science and Technology 36 (2): 227–38. https://doi.org/10.1080/027868202753504083.

Myhre, G., D., F.-M. Shindell, W. Breon, J. Collins, J. Fuglestvedt, D. Huang, J.-F. Koch, D. Lamarque, B. Lee, and T. Mendoza. 2013. "2013: Anthropogenic and Natural Radiative Forcing." In *Climate Change 2013: The Physical Science Basis. Contribution of Working Group I to the Fifth Assessment Report of the Intergovernmental Panel on Climate Change*, 659–740. Cambridge University Press.

Olfert, J.S., and N. Collings. 2005. "New Method for Particle Mass Classification—the Couette Centrifugal Particle Mass Analyzer." *Journal of Aerosol Science* 36 (11): 1338–52. https://doi.org/10.1016/j.jaerosci.2005.03.006.

Olfert, J.S., K.StJ. Reavell, M.G. Rushton, and N. Collings. 2006. "The Experimental Transfer Function of the Couette Centrifugal Particle Mass Analyzer." *Journal of Aerosol Science* 37 (12): 1840–52. https://doi.org/10.1016/j.jaerosci.2006.07.007.

Park, K., D. B. Kittelson, and P. H. McMurry. 2003. "A Closure Study of Aerosol Mass Concentration Measurements: Comparison of Values Obtained with Filters and by Direct Measurements of Mass Distributions." *Atmospheric Environment* 37 (9–10): 1223–30. https://doi.org/10.1016/S1352-2310(02)01016-6.

Peck, Jay, Oluwayemisi O. Oluwole, Hsi-Wu Wong, and Richard C. Miake-Lye. 2013. "An Algorithm to Estimate Aircraft Cruise Black Carbon Emissions for Use in Developing a Cruise Emissions Inventory." *Journal of the Air & Waste Management Association* 63 (3): 367–75. https://doi.org/10.1080/10962247.2012.751467.

Rawat, V. K., D. T. Buckley, S. Kimoto, M. Lee, N. Fukushima, and C. J. Hogan. 2016. "Two Dimensional Size–mass Distribution Function Inversion from Differential Mobility Analyzer–aerosol Particle Mass Analyzer (DMA–APM) Measurements." *Journal of Aerosol Science* 92 (February): 70–82. https://doi.org/10.1016/j.jaerosci.2015.11.001.

SAE. 2011. "Aircraft Gas Turbine Engine Exhaust Smoke Measurement," July. https://doi.org/10.4271/ARP1179D.

SAE. 2013. "Procedure for the Continuous Sampling and Measurement of Non-Volatile Particle Emissions from Aircraft Turbine Engines," November. https://doi.org/10.4271/AIR6241.

Sakurai, H., K. Park, P. H. McMurry, D. D. Zarling, D. B. Kittelson, and P. J. Ziemann. 2003. "Size-Dependent Mixing Characteristics of Volatile and Nonvolatile Components in

Diesel Exhaust Aerosols." *Environmental Science & Technology* 37 (24): 5487–95. https://doi.org/10.1021/es034362t.

Schauer, J. J., B. T. Mader, J. T. DeMinter, G. Heidemann, M. S. Bae, J. H. Seinfeld, R. C. Flagan, et al. 2003. "ACE-Asia Intercomparison of a Thermal-Optical Method for the Determination of Particle-Phase Organic and Elemental Carbon." *Environmental Science & Technology* 37 (5): 993–1001. https://doi.org/10.1021/es020622f.

Schindler, W., C. Haisch, H. Beck, R. Hiessner, E. Jacob, and D. Rothe. 2004. "A Photoacoustic Sensor System for Time Resolved Quantification of Diesel Soot Emissions." *SAE Technical Paper 2004-01-0968*.

Schulz, C., B.F. Kock, M. Hofmann, H. Michelsen, S. Will, B. Bougie, R. Suntz, and G. Smallwood. 2006. "Laser-Induced Incandescence: Recent Trends and Current Questions." *Applied Physics B* 83 (3): 333–54. https://doi.org/10.1007/s00340-006-2260-8.

Seinfelf, John H., and Spyros N. Pandis. 1963. *Atmospheric Chemistry and Physics : From Air Pollution to Climate Change /*. Third edition. http://lib.myilibrary.com/detail.asp?ID=909410.

Smith, Jon, Marc Lipsitch, and Jeffrey W. Almond. 2011. "Vaccine Production, Distribution, Access, and Uptake." *The Lancet* 378 (9789): 428–438.

Snider, Graydon, Crystal L. Weagle, Kalaivani K. Murdymootoo, Amanda Ring, Yvonne Ritchie, Emily Stone, Ainsley Walsh, et al. 2016. "Variation in Global Chemical Composition of $PM_{2.5}$: Emerging Results from SPARTAN." *Atmospheric Chemistry and Physics* 16 (15): 9629–53. https://doi.org/10.5194/acp-16-9629-2016.

Steel, Nicholas. 2016. "Global, Regional, and National Comparative Risk Assessment of 79 Behavioural, Environmental and Occupational, and Metabolic Risks or Clusters of Risks, 1990–2015: A Systematic Analysis for the Global Burden of Disease Study 2015." *The Lancet* 388 (10053): 1659–1724.

Stettler, Marc E.J., Adam M. Boies, Andreas Petzold, and Steven R.H. Barrett. 2013. "Global Civil Aviation Black Carbon Emissions." *Environmental Science & Technology*, August, 130823150610008. https://doi.org/10.1021/es401356v.

Stipe, Christopher B., Brian S. Higgins, Donald Lucas, Catherine P. Koshland, and Robert F. Sawyer. 2005. "Inverted Co-Flow Diffusion Flame for Producing Soot." *Review of Scientific Instruments* 76 (2): 023908. https://doi.org/10.1063/1.1851492.

Stolzenburg, M. R., and P. H. McMurry. 2008. "Equations Governing Single and Tandem DMA Configurations and a New Lognormal Approximation to the Transfer Function." *Aerosol Science and Technology* 42 (6): 421–32. https://doi.org/10.1080/02786820802157823.

Stratmann, F., Th. Kauffeldt, D. Hummes, and H. Fissan. 1997. "Differential Electrical Mobility Analysis: A Theoretical Study." *Aerosol Science and Technology* 26 (4): 368–83. https://doi.org/10.1080/02786829708965437.

Symonds, J. P. R., K. St.J. Reavell, and J. S. Olfert. 2013. "The CPMA-Electrometer System—A Suspended Particle Mass Concentration Standard." *Aerosol Science and Technology* 47 (8): i–iv. https://doi.org/10.1080/02786826.2013.801547.

Tilmes, Simone, Rolf Bee, and Ross Salawitch. 2008. "The Sensitivity of Polar Ozone Depletion to Proposed Geoengineering Schemes." *Science* 320 (5880): 1201–4. https://doi.org/10.1126/science.1153966.

Appendices

Appendix A: Effects of Multiple charges

The analysis used above to determine the transfer function of the CPMA relies that the aerosol is only singly charged however, the charge neutralizer used in a DMA has the potential to impart multiple charges on each particle. The likelihood of having multiple charges on a single particle is based on the particle diameter, and the aerosol temperature and pressure. Larger particles are more likely to be multiply charged when compared to smaller particles. Figure A.1 displays the normalized particle distribution that is leaving the DMA. The figure was generated by applying the transfer-function of the DMA to the overall particle distribution while assuming a charge from 1 to 5 on the particle. The results are also scaled based on the likelihood of a charge neutralizer to impart a number of charges onto a particle of known diameter. Initial SMPS scans of the particle distribution displayed the count median diameter (CMD) was 70.44 nm with a geometric standard deviation (GSD) or 1.76.

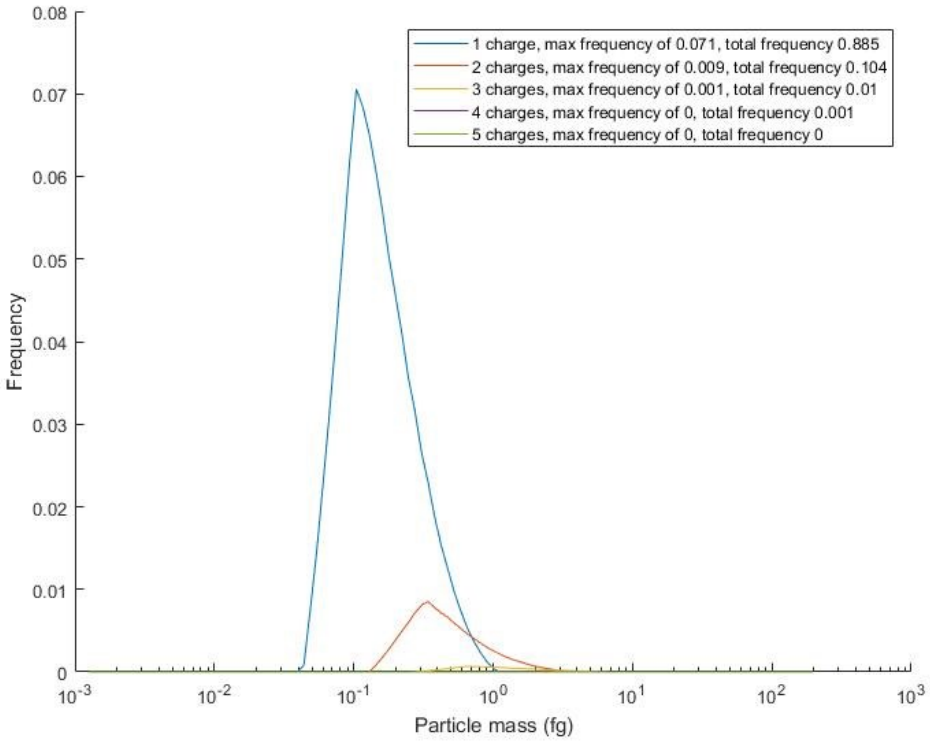

Figure A.1: Frequency of particles leaving the DMA for a set point of 0.1 fg with an aerosol flow rate of 1.5LPM and sheath flow of 2LPM.

Figure A.1 displays how rapidly the particle frequency drops off when multiple charges are considered. It can be found that particles are 9 times more likely to have 1 charge relative to 2, while 1 charge is 100 times more likely than 3, at a set point of 0.1 fg. This aerosol represents the particles leaving the DMA, as such, the frequency of multiple charges will drop even further after passing through the first CPMA. Figure A.2 displays the theoretical aerosol that is leaving the first CPMA. At these set points (aerosol flow rate of 1.5 LPM, DMA sheath flow 2 LPM, CPMA resolution of 3 and specific mass set point of 0.1 fg), there are no multiply charged particles leaving the CPMA. These values are dependent on the set points of the various devices.

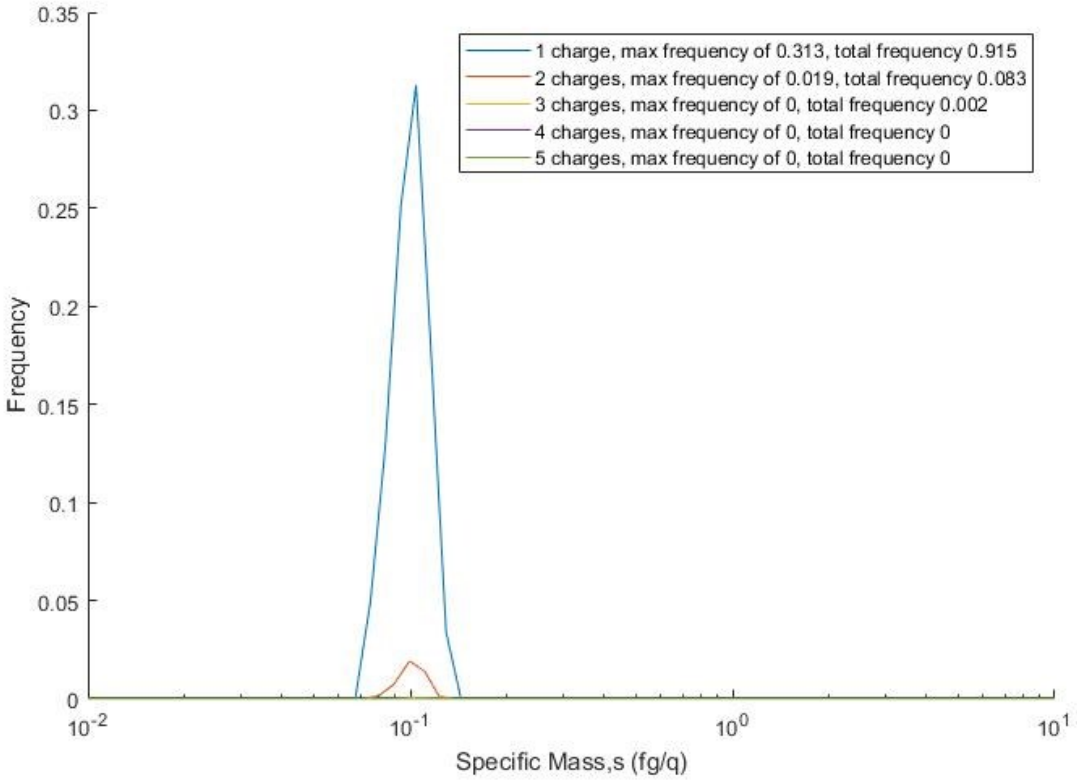

Figure A.2: Theoretical aerosol leaving upstream CPMA with set point 0.1 fg, resolution of 10 and aerosol flow rate of 0.3 LPM.

Examining every setpoint that was used in experimentation reveals the worst case scenario to be at aerosol flow of 4LPM, DMA sheath flow of 5LPM, CPMA specific mass setpoint of 1fg and resolution of 3. At these conditions 89.4% of particles have 1 charge, 10% will have 2 and 0.6% will have 3 charges when leaving the first CPMA (a full summary of all data points examined can be seen in Table A.0.1). With a limited number of multiply charged particles in the system, the effect on the fit of the transfer function and thus the three fit parameters will have little effect.

Table A.0.1: Frequency of multiple charges for various set points used for testing.

Flow Rate (LPM)	Particle Mass (fg)	Resolution	Frequency		
			1 Charge	2 Charges	3 Charges
0.3	0.01	3	0.993	0.007	0
0.3	0.01	5	0.994	0.006	0
0.3	0.01	10	0.999	0.001	0
0.3	0.1	3	0.991	0.009	0
0.3	0.1	5	0.995	0.005	0
0.3	0.1	10	1	0	0
0.3	1	3	0.998	0.002	0
0.3	1	5	1	0	0
0.3	1	10	1	0	0
0.3	10	3	1	0	0
0.3	10	5	1	0	0
0.3	10	10	1	0	0
0.3	100	3	1	0	0
0.3	100	5	1	0	0
0.3	100	10	1	0	0
1.5	0.01	5	0.959	0.041	0
1.5	0.1	3	0.915	0.083	0.002
1.5	0.1	5	0.911	0.087	0.002
1.5	0.1	10	0.88	0.116	0.003
1.5	1	3	0.903	0.093	0.004
1.5	1	5	0.908	0.089	0.004
1.5	1	10	0.935	0.062	0.003
1.5	10	3	0.893	0.107	0
1.5	10	5	0.893	0.107	0
1.5	10	10	0.889	0.111	0
4	1	3	0.894	0.1	0.006
4	1	5	0.899	0.095	0.006
4	1	10	0.922	0.072	0.007
4	10	3	0.88	0.12	0.001
4	10	5	0.881	0.118	0.001

Appendix B: Summary of Repeatability data for the CPMA

The repeatability of the CPMA was found in chapter 3. A figure presented all of the data for these measurements and the raw data was not given. Table B.0.2 contains the raw data used to generate this figure.

Table B.0.2: Repeatability measurements for the CPMA.

Date	Flow Rate (LPM)	Resolution	Mass Set point (fg)	Repeatability	Device
11-Aug	1.50	5	1	0.00489	CPMA A
19-Aug	1.50	5	0.1	0.02510	CPMA A
19-Aug	1.50	5	1	0.00165	CPMA A
19-Aug	1.50	5	10	0.00098	CPMA A
6-Sep	1.50	3	0.1	0.01304	CPMA A
6-Sep	1.50	3	1	0.00488	CPMA A
6-Sep	1.50	3	10	0.00611	CPMA A
6-Sep	1.50	3	100	0.01740	CPMA A
7-Sep	0.30	3	0.1	0.00922	CPMA A
7-Sep	0.30	3	1	0.00215	CPMA A
7-Sep	0.30	3	10	0.00349	CPMA A
7-Sep	0.30	3	100	0.01461	CPMA A
7-Sep	0.30	5	100	0.01660	CPMA A
8-Sep	0.30	5	0.1	0.00487	CPMA A
8-Sep	0.30	5	1	0.00215	CPMA A
8-Sep	0.30	5	10	0.00321	CPMA A
9-Sep	0.30	10	1	0.00232	CPMA A
9-Sep	0.30	10	10	0.00341	CPMA A
12-Sep	1.50	10	1	0.00256	CPMA A
12-Sep	1.50	10	10	0.00363	CPMA A
20-Nov	4.00	3	1	0.00244	CPMA A
20-Nov	4.00	3	10	0.00170	CPMA A
20-Nov	4.00	5	1	0.00153	CPMA A
20-Nov	4.00	5	10	0.00267	CPMA A
20-Nov	4.00	10	1	0.00184	CPMA A
13-Sep	0.30	3	0.1	0.01069	CPMA B
13-Sep	0.30	3	1	0.00746	CPMA B
13-Sep	0.30	3	10	0.00278	CPMA B
15-Sep	1.50	3	1	0.00134	CPMA B
15-Sep	1.50	3	10	0.00140	CPMA B
15-Sep	1.50	3	100	0.01093	CPMA B

15-Sep	1.50	5	1	0.00232	CPMA B
15-Sep	1.50	5	10	0.00865	CPMA B
15-Sep	1.50	5	100	0.01080	CPMA B
15-Sep	1.50	10	1	0.02002	CPMA B
15-Sep	1.50	10	10	0.00372	CPMA B
17-Nov	0.30	5	0.1	0.01451	CPMA B
17-Nov	0.30	5	1	0.00651	CPMA B
17-Nov	0.30	5	10	0.00277	CPMA B
18-Nov	0.30	5	100	0.01887	CPMA B
18-Nov	0.30	10	10	0.00420	CPMA B
18-Nov	0.30	10	100	0.05914	CPMA B
19-Nov	4.00	3	1	0.00298	CPMA B
19-Nov	4.00	3	10	0.00208	CPMA B
19-Nov	4.00	5	1	0.00146	CPMA B
19-Nov	4.00	5	10	0.00245	CPMA B
19-Nov	4.00	10	1	0.00094	CPMA B

Appendix C: Summary of Repeatability data for the Faraday cup-electrometer testing

The repeatability of the Faraday cup-electrometer test was found though the use of the data used to determine the lines of best fit. The generalized equation to calculate the expected value for both systems from the data is as follows:

$$Expected\ value = \frac{Data\ of\ System\ 1 + Data\ of\ System\ 2}{2}$$

This procedure of calculating the expected value was used for all data points. The distance from this expected value was found then normalized. A summary of all of the data can be seen below in Table C.3.

Table C.3: Farady cup-electrometer repeatability data

Date	System 1	System 2	Expected Value	Normalized Difference		Device Intermediate Precision
				System 1	System 2	
Jan-21	8.116	8.706	8.411	-0.035	0.035	0.008
	7.289	7.606	7.447	-0.021	0.021	
	5.442	5.623	5.533	-0.016	0.016	
	4.317	4.505	4.411	-0.021	0.021	
	3.171	3.324	3.247	-0.023	0.023	
	2.111	2.212	2.162	-0.023	0.023	
	1.029	1.050	1.040	-0.010	0.010	
Jan-22	7.972	8.299	8.136	-0.020	0.020	0.002
	6.930	7.300	7.115	-0.026	0.026	
	6.068	6.355	6.212	-0.023	0.023	
	5.089	5.361	5.225	-0.026	0.026	
	4.149	4.339	4.244	-0.022	0.022	
	3.086	3.236	3.161	-0.024	0.024	
	2.032	2.119	2.076	-0.021	0.021	
	0.958	1.003	0.980	-0.023	0.023	
Jan-25	7.568	7.861	7.715	-0.019	0.019	0.004
	6.560	6.881	6.720	-0.024	0.024	
	5.655	5.973	5.814	-0.027	0.027	
	4.706	4.977	4.842	-0.028	0.028	
	3.842	4.003	3.923	-0.020	0.020	
	2.861	2.968	2.915	-0.018	0.018	
	1.840	1.916	1.878	-0.020	0.020	
	0.873	0.900	0.887	-0.015	0.015	
Jan-26	6.932	7.217	7.074	-0.020	0.020	0.005
	5.983	6.216	6.100	-0.019	0.019	
	5.205	5.376	5.291	-0.016	0.016	
	4.331	4.512	4.421	-0.021	0.021	
	3.459	3.627	3.543	-0.024	0.024	
	2.594	2.664	2.629	-0.013	0.013	
	1.671	1.705	1.688	-0.010	0.010	
	0.715	0.746	0.730	-0.021	0.021	